We thank the three reviewers for reading the manuscript so carefully and providing detailed and very valuable comments which helped to improve the manuscript substantially. We have carefully considered all comments and changed the manuscript accordingly. Please find our detailed point-to-point replies below in italic and blue.

Anonymous Referee #1

This manuscript shows a case-study wherein Raman lidar data is used to derive second through fourth order moment statistics of temperature throughout the convective boundary layer and in the interfacial layer. Overall, the authors describe well how the statistics are computed, including an analysis of the significant errors from the noisy lidar data. The results are discussed well and the authors consider the large errors in their interpretation of the data. The method outlined in the paper, using Raman lidar measurements, will allow investigation of various boundary layer questions, which the authors lay out within the conclusions. The manuscript is well-written overall and data is generally good.

We thank the reviewer for these positive comments.

However, there are some questions over the application of the power law, which is the crux for many of the derived higher order statistics. In order to address this question, and several other minor points listed below, additional analysis may need to be performed leading to major revisions.

We have addressed all these points in the revised version as detailed below.

Specific Comments

Title: The title should be “Profiles of second- to fourth-order moments of . . .”

Thanks, we have changed the title as suggested.

p. 29022 Line 1: Martin et al. (2014) used UAS to identify and examine process in the entrainment zone, which should be referenced here and invalidates part of this sentence. However, UAS of course cannot continuously examine it due to a short endurance (among other issues).

We have included the reference and rewritten the text.

p. 29022 Line 10: There should be more information about the Kadygrov et al. study here, as this sentence seems incomplete. How did the thermal turbulence characteristics compare with the expected power-law within the lowest 200 m?

Information added.

p. 29026 Line 28: What is meant by “is not necessarily the case for the other cases”? What are the other cases?

Rewritten in order to avoid misunderstandings; we just wanted to stress that we discuss a case study. The reviewer misunderstood “the other cases” while only “other cases” was written.

p. 29026 Line 29: Seems like several words (or variable) were left out. Should it be '. . . the height of maximum dT/dz agrees. . . while the height of the maximum gradients from the radiosonde is about 60 m lower'?

Yes, thanks. Rewritten.

p.29027 Line 13: Was the detrending performed for time series of temperature at each separate height? Should clarify.

Clarified. A linear regression was applied at all heights. However, due to the absence of strong mesoscale variability in this case, the effects of the linear regression are minor and it would also have been appropriate just to subtract the mean values at each height.

p. 29028, line 12: What is the power-law fit? It should be provided within the present manuscript for clarity. Does this refer to Eq. 32 in Lenschow et al. (2000)?

Clarified, we were referring to the shape of the structure function in the inertial subrange, which translates in a tau^(2/3) functional dependence around lag zero. We are now used the term "structure function" in order to avoid confusion with spectral analysis. Thus, it indeed refers to Eq. 32 of Lenschow et al. (2000).

p. 29028, line 20: Why was the interval of -200 – 200 s chosen for extrapolation of the power law fit? If Eq. 32 from Lenschow et al. (2000) was used, the power law fit was derived using the inertial subrange hypothesis. With independent temperature samples of 10-s, it is unlikely that the resolved temperature fluctuations are due to turbulence within the inertial subrange. For much of the time period of -200 – 200 s that is used for the fitting, the ACF shown in Fig. 6 is negative and near zero, which would indicate that the fluctuations of temperature are from turbulent motions outside of the inertial subrange. By fitting the curve to data outside of the inertial subrange, the estimate of the noise would tend to be too high, making the temperature variance underestimated.

The reviewer is raising important and substantial questions. We agree that the procedure for determining the integral scale and the separation of noise and atmospheric variances should be explained in more detail. We inserted a new paragraph at the end of section 3.2 to do this.

*The determination of the integral scale and the variances is in principle an iterative process. First of all, we are using a standard number of fitlags to determine the integral scale profile. Then, we are using the knowledge that the zero crossing of the structure function is theoretically at 2.5 * integral scale. In principle, this can be executed at each height level. However, we could interrupt this iteration after the first step using a mean value of the integral scale of about 80 s leading to 15 fitlags or 150 s as "safe" compromise. The remaining sensitivity of changing the number of fitlags between 10 and 20 is less than the estimation of the noise and sampling error bars. A similar approach is used for separating the noise in the higher-order moments. However, whereas we are using the same number of fitlags here we are using a linear extrapolation due to lack of knowledge of the higher-order structure function.*

Based on these results and following this comment of the reviewer and a similar comment of reviewer 2, we exchanged the previous results obtained with a turbulence analysis over 20 lags (corresponding to 200 s) against the results obtained with a turbulence analysis over 15 lags (corresponding to 150 s). As mentioned above, the differences between the results are within the error bars which are given

anyway with all the results. Thus we can conclude that the selection of the fitting region is not critical (which is also illustrated with the example of the fitting function shown in the new figure 6c). Nevertheless, this fitting region indeed corresponds better to the integral scales.

Please note that with absence of mesoscale variability the temperature fluctuations determined in the ACF from lag 0 to the first zero crossing are indeed due to turbulence in the inertial subrange. This is due to the fact that the integral scale is larger than the temporal resolution of our lidar system and the fit to the structure function looks just perfect.

We admit (also in the revised version of the manuscript) that further refinements are possible by using different fit intervals for different heights. However, this has not yet been made within any previous study (using Doppler lidar data or humidity lidar data) – to the best of our knowledge.

p. 29032, Section 3.5: It would be beneficial to compare how the magnitude of the temperature variance within the CBL compares to those measured in other studies in similar environments. While it would be difficult to compare actual values, it would be beneficial to show if those measured within this study were of the same magnitude as those measured using in-situ measurements.

We added a brief discussion at the end of section 3.5. For quantitative comparisons, often normalization of the temperature variance profile with T is used. But in the real world with its heterogeneous land-use and corresponding flux variability such scaling becomes difficult. Instead of a value at the lidar site, one could employ several flux stations and try to find a more representative scaling parameter by weighted averaging of the measurements made over different land-use types. But even then one expects that the scaled temperature variance profile depends on the ratio of the mean entrainment and surface. Thus, we decided not to scale the variance profile here and leave further generalizations to future studies based on more cases.*

Conclusions: Overall, the conclusions were well-supported by the data presented and were well written. It may be better to highlight some of the key findings with it by using a bulleted list, though.

We thought about this suggestion but decided instead to structure the text with more paragraphs so that we can directly comment on the results.

p. 29037, line 12: By collecting data closer to the ground, it may also be possible to compare measurements to high-quality in-situ sensors, at least at one location. Although that is outside of the scope of this paper, I would recommended doing comparisons with a fast-response thermistor mounted on a tower, if possible. Statistics from the in-situ sensor could be compared with those from the RRL using this technique. This would better allow for quantification of errors, and for assessing how this method could possibly be improved for accurately measuring temperature variance and other higher order statistics.

Thanks. We fully agree. Such comparisons are certainly planned in future studies.

Figure 3: The profile of temperature should be removed, as it provides no additional information. Within the text, any discussion that uses the temperature profile could be made with the potential temperature profile instead.

The temperature profile is the primary data product. Thus, we prefer to keep this plot for clarity. We have added a corresponding comment to the text.

Figure 4: There should be errorbars for the statistics from the 1100-1200 time period as well.

OK, added.

Figure 5: Again, showing only either the potential temperature or temperature crosssections is sufficient, do not need to show both. I would learn towards showing potential temperature, as the top of the CBL is shown better. In the temperature fluctuation plot, the colorbar would be better if T'=0 were grey, not green, as the more subtle fluctuations would be more visible.

The temperature profile is the primary data product (see above). Thus, we prefer to keep this plot for clarity. We have changed the colorbar of the temperature fluctuation plot so that the fluctuations are now seen much better - thanks.

Figure 6: Including the fit of the power-law to the data on the graph (at least for one height) would be useful, so that the goodness of the fit is shown.

Good idea, added (see new Fig. 9c).

Technical Corrections

P. 29021 Line 27: In citation, year should be 2011. Should check other citations to make sure they are all correct, as well. One other incorrect citation was noticed that is listed below.

Thanks, corrected.

P. 29022 Line 1: Should be in-situ sensors

Corrected.

P. 29022 Line 16: Should be Lenschow et al. 2000, not 2010.

Corrected.

P. 29023 Line 20: Should be 'out of', not 'our of'

Corrected.

Additional reference:

Martin S., F. Beyrich, and J. Bange. Observing Entrainment Processes Using a Small Unmanned Aerial Vehicle: A Feasibility Study, Bound.-Lay. Meteorol., 150, 449-467, 2014.

Included.

Anonymous Referee #2

The paper is well written the results are new and unique.

We thank the reviewer for these positive comments.

Nevertheless there are some points which need clarification and may lead to a change of results.

We have clarified all points in the revised version.

Main points:

* the authors use the method of Lenschow et al (2000) to derive statistical parameters from the (inherently) noisy data of a Raman Lidar. Within this method the autocorrelation functions of different order have to be extrapolated to lag zero to remove components generated by noise in the data. At least for the variance a power law function deduced from Kolmogorov scaling is used. Kolmogorov scaling is only valid in the inertial subrange but it is not ensured that this is the case. I therefore recommend a re-calculation which will probably give different results.

We agree with the reviewer that these aspects should be explained more in detail. Some refinements beyond the strategy explained in Lenschow et al. (2000) were missing in the literature yet. See our detailed reply to the similar comment of reviewer 1 (on page 2 of this document) in which we explain how we selected the fitting region and that we reanalyzed the data with 15 lags for the revised version.

* the derived Skewness profile shows within the boundary layer values around zero and accordingly deviates substantially from what is usually found in LES simulations, aircraft or other experimental data (e.g. Mironov et al 1999, fig. 1). As in the middle of a common convective boundary layer rising plumes of warm air are narrow and surrounded by large areas of air close to the average temperature the skewness can be expected to be positive. This deviation should be discussed.

Thanks, we adapted the discussion in section 3.6. The reference had already been included in the previous version. We agree that one expects to find typically positive temperature skewness in the CBL but this may be small depending on the strength of turbulence and of the inversion. Actually, the reference shows skewness values between 0 and 2 inside the CBL and a negative peak at the CBL top. Our results are thus in good agreement with this taking the statistical errors (see error bars) into account.

* A comparison with airborne measurements, LES results or parameterizations from the literature is missing.

As suggested, we extended the comparisons with literature data. We have unfortunately not yet simultaneous airborne data to compare our results with. Comparisons with LES for the same case are in preparation but require an extensive discussion of the LES configuration which is beyond the scope of this manuscript.

Details:

3.1 Data set

page 29025: Some information about general meteorology (wind, minimum and maximum temperature, surface fluxes, etc.) would be nice.

Added.

page 29025, line 14: „β_{par} was measured with the rotational Raman lidar technique by use of a temperature-independent reference signal." please explain or give a reference.

Reference added.

p. 29026, l.1. calibration

There are missing some details of the calibration: is one factor for the whole height range derived, or several for different height intervals. How large is the uncertainty in the calibration factor (called ∂T/∂Q in equation 5 below).

We have clarified that the calibration is the same for all heights. The uncertainty of the calibration is difficult to estimate but if we assume that it depends mainly on the calibration of the radiosonde, the uncertainty is < 0.2 K (according to the manufacturer, see http://www.graw.de/home/products2/radiosondes0/radiosondedfm-090/). We have added also this information.
But please note that the measured temperature fluctuations do not depend on the absolute accuracy of the temperature measurements but on its relative accuracy. Even with an error of 1 K, the relative accuracy is thus better than (1 K)/(250 K) = 0.4 %.

p. 29026, l. 23. ... the potential temperature (...) [profile] is nearly constant ... fig. 3 ... Just a remark: around 800m is a region with stable stratification. For the radiosonde one could assume that it entered a plume with warmer air, but i am wondering why it is also visible in the RRL data even in the one hour average (see also the gradient profile in fig 4). Around that height is also a minimum in variance (fig 9) and skewness (fig 10) - any comments on that ?

Thanks for looking so closely to the data! We thought about this point quite a while but it seems to us that this step of 0.5 K in the mean CBL temperature profile is not important for the higher-order-moment profiles. One could guess that a stable lid reduces the variance by slightly damping the exchange. But this hypothesis seems too vague to us. Furthermore, 800 m a.g.l. corresponds to 0.65 z_i. The variance minimum is lower and the skewness profile (both previous and new one) do not show significant features taking the error bars into account at this height. Just the minimum in the variance profile affects the skewness profile at 0.6 z_i. as it is used for the normalization of the TOM profile when calculating skewness. So we decided not to extend the discussion to this point.

3.2 Turbulent temperature fluctuations

p. 29027, l.9., eq. 1 There is missing a time dependence in the equation. And it is not clear whether the trend is equal for all levels. To additionally include the trend removal one may write:

$$T(z,t) = \overline{T}(z) + a(z) * (t - t_m) + T'(z,t)$$

where the overbar denotes a linear temporal average operator which fulfills the Reynolds averaging rules (e.g. Wyngaard 2010), a is the trend, etc. ...

Clarified. The trend is equal for all heights for our case. We have also added the reference. We decided not to change the equation as all necessary information is already given in the text.

p. 29027, l.12. "... a linear fit to the temperature time series was sufficient due to the quasi-stationary state of the CBL ..." In a quasi stationary turbulent medium parameters like mean and variance of a variable are constant although the variable itself is fluctuating. If it is necessary to remove a temporal trend, no matter whether linear, quadratic, sinusoidal or whatever, it is strictly speaking not stationary any more. Please reformulate. Were there any objective methods applied to ensure that the dataset is quasi stationary?

Rewritten as suggested. We decided to drop the criticized term "quasi-stationary".

p. 29028, l. 12: "By calculation of the autocovariance function (ACF) of a variable and extrapolating the function to zero lag with a power-law fit ..." This probably refers to equation 32 in Lenschow et al (2000) which can be written as $A(\tau) = \overline{T'^2} - C \cdot \tau^{2/3}$ with lag τ. At least it is mentioned further down (p.29032) that the exponent in the power law is 2/3. This power law with an exponent of 2/3 for A(τ) stems from Kolmogorovs structure function and is only valid in the intertial subrange i.e. at scales clearly smaller than those of the external forcings and larger than those of viscosity. This becomes obvious as for large lags A(τ) becomes increasingly negative although one would expect that the autocovariance (i.e. the autocorrelation multiplied by the variance) asymptotically tends to zero. As an indicator for the scale where the Kolmogorov ACF becomes invalid could serve the zero intercept of the measured ACF.

The ACF is fitted to lags up to 200s (p.29028, l. 19) which can be related to a length scale of 2km by assuming a horizotal wind of 10 m/s. This is clearly larger than the height of the convective BL (1.23km) which can be regarded as the length scale of the external forcing. Thus A(τ) is applied to regions outside the intertial subrange. I recommend to reduce the range of lags to which the ACF is fitted. Otherwise I would recommend to fit a function which aproximates asymptotically zero for large lags and which is not restricted to the interital subrange. I expect that this will change especially the integral timescale but also the other estimated parameters.

This is a very good point. We agree that this issue must be explained more in detail. Finally, structures of the ACF closer to the zero crossing are clearly due to turbulence in the inertial subrange because the fit of the structure function works very well at each height. Furthermore, the integral scale is larger than the temporal resolution of the lidar at all heights. See our detailed reply to the similar comment of reviewer 1 (page 2). But please note that comparisons with the CBL height and integral length scales (using horizontal wind data) are only rough estimates. The integral time scale times 2.5 directly gives the zero crossing of the ACF. We have reanalyzed the data now with 15 lags for the revised version.

p. 29028, l. 14.:

"Alternatively, one may calculate the power spectrum of the fluctuations and use Kolmogorows −5/3 law within the inertial subrange in order to determine the noise level." Description is a somewhat vague. The method is e.g. described and investigated in O'Connor et al 2010.

We added this reference.

Allthough the authors do not use the spectral method to correct for the noise in the data it would be interesting to see powerspectra of the data as they show an independent measure of noise.

We decided not to include the power spectra to the manuscript because we do not use them. Please note that the noise level in the power spectra is larger because of the conversion to the frequency space and thus the ACF method is preferred (see section 3.2, end of second last paragraph). But as the reviewer is interested we show the spectra here for three selected heights:

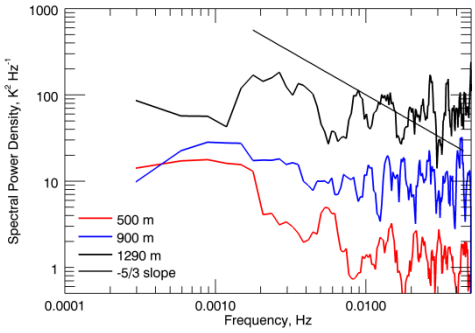

3.3 Noise errors

p. 29029, l. 9: "The comparison confirms that the photon shot noise gives the main contribution and that other statistical error sources are comparatively small." If i estimate correct from fig. 7 the Poisson statistics account for about 75% of the error. Where do the remaining 25% come from ?

Explanation added to the revised version. We assume that electric noise in the analog signals is responsible for most of the remaining noise.

p. 29029, l. 17: "... analog signals and not photon-counting signals have been used ..." I understand what analog signals are but i do not understand what the additional not photon-counting signals are, please specify.

Clarified: "... analog signals have been used" and photon-counting signals have not been used...

p. 29030, l. 11, eq. 6: I would find it more didactically to start with the basic retrieval equation to come to the error estimate.

OK. Modified as suggested.

p. 29030, l. 5, eq. 5: This means that the calibration constant $\partial T/\partial Q$ is assumed to have a negligible uncertainty. Is this reasonable ?

Yes, we have detailed this in the revised version.

p. 29031, l.11: If i understand right the uncertainty estimate given in eq. 10 does not represent the dominating part of the error propagation. Would it not be more meaningful to write the equation in

a way including this important part ? This would also clarify why error profiles for different temporal and spatial resolutions can be derived by a simple scaling from the 10s/109m profile.

We clarified this point. Equation 10 describes the scaling of the statistical errors with temporal resolution, range resolution, system efficiency and telescope area etc.; it does not neglect any parts of the error propagation.

3.4 Integral scale

p. 29032, l.7: The variance at z/zi is close to zero because the noise estimate by the Lenschow et al. (2000) method attributes all the observed variance as noise. I would expect that the temperature variance inside a convective BL would never go to zero. Thus probably the noise removal method does not work properly. Please reformulate the sentence.

Rewritten.

p. 29032, l. 10.: "The integral scale shows values between (40±22) s and (122±12) s in the CBL." These values are smaller than the 200s maximum lag used to fit the theoretical ACF. The integral scale is sometimes interpreted as the size of the energy containig eddies, accordingly the ACF has been fitted to regions beyond the inertial subrange. Interestingly is that below 800m, the height of the small stable layer, in average larger time scales appear - any idea ?

We added a brief discussion of this question. Please note that the integral time scale times 2.5 gives the zero crossing of the ACF (see detailed reply to similar point of reviewer 1 on page 2). Thus the integral scale is only 0.4 times the maximum lag which can be used.

p. 29032, l. 10.: "The integral time scale (which can be related to a length scale ..." It would be great if this could be done. These derived Length scales could be compared to length scales derived e.g. from LES (e.g. ed Roode et al. 2004, fig. 5 and 6, or Moeng and Wyngaard 1989)

We decided not do to so here as we believe that this discussion is beyond the scope of this manuscript and there is anyway significant uncertainty when using horizontal wind data of the radiosonde. We plan to compare the results with dedicated LES simulations for this case in the near future.

3.5 Temperature variance

p. 29032, l.23: sampling and noise error are probably determined by the method of Lenschow et al. (2000). This should be mentioned here or in the description of the method above. The different meaning of these two error estimates should be explained.

We added explanations. Indeed, we used the method of Lenschow et al (2000) also for deriving all errors.

p. 29033, l.5: The variance profile could be compared with profiles found in the cited literature. Especially with parameterizations as e.g. mentioned in Moeng and Wyngaard (1989). The latter also assumes a relation to the surface to entrainment flux ratio.

Certainly, these are important next steps. But as discussed above, we believe that such comparisons require extensive discussion of also of the LES configuration which we plan to do in future studies.

3.6 Third-order moment and skewness

p. 29033, l. 11, eq. 11: Are skewness and TOM really determined directly from the measured temperature time series? Or is here also the method from Lenschow et al. 2000 applied? The latter corrects for the skewness of the (Poisson) noise which i would expect to be nonzero. Please clarify.

Clarified. Also for the TOM and S, we applied the method of Lenschow et al. 2000.

p. 29033, l. 17: "Up to about 0.9 zi , TOM was not different to zero ..." This is somewhat astonishing if one takes into account the structure of the turbulence in the CBL: rising warm plumes are preferably narrow or organized along the borders of hexagonal cells (see e.g. Taeumner et al 2014). They are surrounded by large areas of air close to the average temperature. This results in positive Skewness as also can be seen in e.g. Mironov et al. (1999), fig. 1 which shows data from different sources. Why is this different here ?

We have rewritten the discussion of this point and included the reference (Mironov et al., 1999) which shows skewness values between 0 and 2 inside the CBL and a negative peak at the CBL top. Our results are in agreement with this taking the statistical errors (see error bars) into account. We added a corresponding discussion to the text. Furthermore, we added the reference Träumner et al (now 2015) in the introduction.

3.7 Forth-order moment and kurtosis

p. 29034, l. 17: "Forth-order moment (FOM) is a measure of the steepness of the distribution." Although this seems to be a common interpretation it is somewhat misleading: the larger the Kurtosis the steeper is the slope of the pdf at the sides of its peak. But also the more flat or less steep are its tails.

Correct, clarified.

p. 29034, l. 20, eq. 12: As for the TOM: is the FOM and K calculated with this equation or with the method of Lenschow et al. (2000) which accounts for the FOM of the noise ?

Throughout this study, we used the method of Lenschow et al (2000).

p. 29034, l. 22: K-3 is sometimes called 'excess Kurtosis'.

True, added.

4 conclusion

p. 29037, l. 7: Gryanik et al. (2005) postulate in equation 3 a relation between the fourth order moment, skewness and variance of temperature. Alhough the errors in FOM and K are large it might be interesting to investigate this here. With the same caution one may add some points to their figure 3.

Thanks. We had included this reference already in the conclusions and commented briefly on closure models. We added now a further sentence on this parametrization which was originally suggested in

Gryanik and Hartmann (2002); we added also this reference. We believe, however, that further analyses would require more cases and a detailed discussion which is beyond the scope of this manuscript. But we will keep this relation certainly in mind for future studies.

Figures:

fig. 1.: Caption mentions some elements which are not in the schematic: e.g. OF for optical fiber, L5 and L6...

Thanks, corrected.

fig. 2.:Backscatter shows some structures in the BL: (a) higher backscatter before 11:30 above 800m and (b) increasingly lower backscatter after 11:30 in the lower half). These structures seem to have no relation to the temperature field or show at least much larger scales than the features which are visible in the T' plot (fig. 5). Is there any interpretation ?

We added a brief discussion of this point. We assume that the aerosol number density and size distribution changed due to advection. Please note that the purpose of this plot is to illustrate the determination of the instantaneous CBL heights. Of course, we do not expect to see a one-to-one relation between the structures in the aerosol field and the temperature field.

fig. 3.: Temperature profiles: ranges of the abscissa could be smaller to make differences between the the profiles better visible.

Done (for both panels).

fig. 4.: One may mark the adiabatic temperature gradient to identify stable and instable regions.

Added.

fig.5: I think the temperature plot does not give that much information as it is dominated by the temperature decrease with height. One less subplot would give more room for the others making them easier readable.

We agree that the plots are printed too small in the ACPD file. This should be corrected in the final ACP lay-out. We prefer to keep the temperature plot in order to show the primary data set as it is.

The ranges of all the color scales seem to be larger than the range of displayed temperatures: e.g. nearly all potential temperature values lie in the range 290-305K whereas the color scale goes from 280-310K. Adpating the color scale would make turbulent structures better visible.

Done. We have changed all color scales.

Both ends of the Temperature fluctuations T' color scale are black making it difficult to decide whether a black pixel denotes for +2K or −2K. please change.

Done. Black now denotes T´ < -2 K; yellow T´ > 2 K.

Fluctuations T' in the free troposphere are larger than in the BL, they are probably noise. It might be an idea to remove data (i.e. heights) where noise in the data comprises for more than say 50% of the measured variance.

We prefer to keep this plot as it is in order to show the same height range as the other plots including Fig. 2.

I do not fully understand why there are gaps in fig 5c (i.e. time height section of T0). These gaps seem to be about 10-20sec long and appear about every 3 1/2 minutes or every 21 mesurement. If i interpret this in the way that after 21 timesteps more than 21*10sec have elapsed this would mean that a time step is by 1/21 = 5% longer than 10sec i.e. 10.5sec. This would affect all derived parameters. Please clarify.

Clarified. In the lowest plot, the data were gridded to exact 10 s intervals. This was made in order to ensure that the derived parameters are all correct.

Last sentence of caption is unclear.

Rewritten.

fig 6.: It is not necessary to show the autocorrelation function for negative lags as it must be from its defintion symmetrically (even if you calculate it for negative lags you are multiplying and adding the same numbers). Reducing the abscissa to only positive lags might increase clarity of the plots. It would be great to see at least one fitted ACF-function and an ACF=0 line would be helpful.

We have added the ACF = 0 and lag = 0 lines. We prefer to keep the abscissa as it is in order to show that the ACF is symmetric. We added a new figure 6c illustrating the fit.

The slow fluctuations of ACF around zero for larger lags might be due to some large scale variability in the data. Although such patterns may also occur in ACF from pseudo random generated time series with no longterm variations, it might be worth to think about high-pass filtering of the data.

We decided not to apply additional filtering in this case and just apply linear detrending. We checked the results very carefully and exclude that artefacts are present. It seems to us that the structures appear due to noise. But of course such filtering can be performed in certain cases.

Caption does not explain the second plot.

Explanation added.

fig. 8: "Error bars show the remaining root-mean-square variation of the noise-corrected data" I do not understand - the integral scale of a time series is one value - it does not vary. Please clarify. The same formulation was used in the following figure captions, please adapt accordingly.

Rewritten.

fig. 9: It is a bit surprising to see nearly zero variance in the CBL and even negative (or exact zero) values at 1.4km, especially as the time height section of T' in fig.5 shows variability at these heights. It would be helpful to see the uncorrected variances to get an idea how large the noise in the data is (see e.g. Wulfmeyer et al. 2010).

We have added a comment on this. The noise errors of the data are already shown.

fig. 10 and 11: If TOM, S, FOM and K have been calculated including a noise correction it would be intersting to see the uncorrected profiles (see e.g. to Wulfmeyer et al 2010)

We have added a comment on this (see above). The noise errors of the data are already shown.

The dashed line marking zi is missing in the Kurtosis plot.

We clarified this in the caption. When adding the line, it nearly overlaps with the error bar. So we decided not to include it here.

Technical:

p. 29022 l.8: year in citation Kadygrov must be 2004 - there seem to be several years wrong (Lenschow 2010 inestead of 2000 ...), please check.

Corrected.

p. 29024 l. 12: scanner mirror is anotated BSU (beam steering unit) in fig 1.

Clarified. The BSU consists – among other components – of 2 scanner mirrors.

p. 29024, l. 17: iris = field stop in caption for fig 1 ?

Yes, clarified.

p. 29024, l.30: i guess specification of filters etc. is given in Behrendt et al ...

Clarified. They are given by Hammann et al. (2014), meanwhile accepted and thus Hammann et al. (2015).

p. 29028, l. 4: remove 'or'

Corrected.

p. 29028, l. 5: 'mean temporal average' is a double average ?

Clarified.

References:

Wyngaard 2010, Turbulence in the Atmosphere, Cambridge University Press

O'Connor, E. J., Illingworth, Anthony, J., Brooks, Ian, M., Westbrook, Christopher, D., Hogan, Robin, J., Davies, F., and Brooks, Barbara, J., 2010: A Method for Estimating the Turbulent Kinetic Energy Dissipation Rate from a Vertically Pointing Doppler Lidar, and Independent Evaluation from Balloon-Borne In Situ Measurements, J. Atmos. Ocean. Tech., 27, 1652–1664, doi:10.1175/2010JTECHA1455.1 .

Stephan R. de Roode, Peter G. Duynkerke, and Harm J. J. Jonker, 2004: Large- Eddy Simulation: How Large is Large Enough?. J. Atmos. Sci., 61, 403–421. doi: 10.1175/1520-0469(2004)061<0403:LSHLIL>2.0.CO;2

K. Träumner, Th. Damian, Ch. Stawiarski, A. Wieser, 2014: Turbulent Structures and Coherence in the Atmospheric Surface Layer Boundary-Layer Meteorol, online doi:10.1007/s10546-014-9967-6

Anonymous Referee #3

The paper demonstrates the capability of the UHOH RR lidar to study temperature fluctuations in the CBL. Statistical moments of higher order have been derived including its uncertainties and partially discussed. The paper is well written, results are novel and well presented. I recommend publication in ACP after minor revisions as specified below.

We thank the reviewer for these positive comments.

General comments

A big part of the paper is written in the first person plural. This is not good scientific language and I would like to motivate the authors to use other formulations.

We have re-rewritten the text at several points according to this suggestion of the reviewer. But one should note that the notions on this point differ. While, e.g., in German and French active sentences should indeed be avoided in scientific writing, the situation is different in modern English and several sources explicitly recommend the use of active phrases in order to avoid misunderstanding (see, e.g., http://www.writing.utoronto.ca/advice/style-and-editing/passive-voice, http://www2.le.ac.uk/offices/ld/resources/writing/writing-resources/science).

The approach to characterize the noise of the analog signal with Poisson statistics is not justified. The authors need to provide a justification and a validation of this approach.

Done. We have added additional references. Furthermore, the approach is validated by the comparison of the independent results which on the one hand come from Poisson statistics and on the other hand from the turbulence analysis (see Fig. 7).

The language lacks sometimes precision. Often no distinction is made between an error source (instrument noise or shot noise) and the resulting uncertainty in temperature.

We have clarified this.

Further, the term “Poisson statistics” is heavily overstressed in this work. It is often used as synonym to “instrument noise” even though it is not even clear, whether the instrument noise follows Poisson statistics. This has to be corrected.

Agreed. We have rewritten section 3.3 and the caption of figure 7. Photon shot noise follows Poisson statistics. For Raman lidar, shot noise is the dominant contribution for uncorrelated noise in the signals. Thus the corresponding formulas can be used to approximate the total noise of the lidar signals and then via error propagation the statistical noise of the temperature measurements. But, while shot noise gives the major contribution, the instrumental noise indeed contains additional sources of uncorrelated noise.

Specific comments

P29020, l2: This implies that nighttime measurements are not possible or usually not done. Please comment.

Rewritten; nighttime RRL measurements have much higher performance than daytime measurements.

P29020, l14: What is "noise variance". "Noise" on l4 refers to signal noise. Here it seems to be the fraction of the temperature variance which is due to signal noise. Later in this phrase the authors say "statistical temperature measurement uncertainty based on Poisson statistics". Only for the lidar expert it is obvious, that "Poisson statistics" must refer to the noise of the measurement and for non lidar experts this phrase is quasi incomprehensible. Please be very precise here.

Rewritten.

P29020, l16: How can an agreement confirm a difference? use "comparison" instead of "agreement".

Rewritten as suggested.

P29020, l17: Here and on P29029, "extrapolate" is not the good word for the process. Wouldn't "scale" describe better the data manipulation? Second, here the authors use "extrapolated analog signal", while in the text (P29029) they use "extrapolated count-rates". Reformulate to achieve consistency and the necessary precision in the language.

Rewritten as suggested.

P29021, l24: I doubt that "temperature turbulence" is a correct term?

Rewritten throughout the text.

P29022, l7: While the range resolution is certainly a limitation for this purpose, I disagree that time resolution can be included here. Kadygrov et al. 2003 (not 2011) used a scanning radiometer, which reduces the time resolution. Multichannel MWR's can do profiling at a much higher time resolution. Further, what do the authors mean with "time dependent errors"? All remote sensing instruments have uncertainties that depend on the atmospheric conditions and hence on time.

Agreed. We have rewritten the text accordingly and the year of the reference.

P29022, l13: The achievements in a better understanding of boundary layer processes based on the radar technology (active remote sensing) needs to be briefly reviewed here (e.g. Jacoby-Koaly et al. 2002, Boundary Layer Meteorology, 103, 361-389, and references therein).

We have added references to radar studies (see introduction). However, the reference which the reviewer is giving does not exist – we assume that she/he means B. Campistron et al., 2002, BLM, 103, 361 - 389.

P29023, l19: ++Raman++ backscatter spectrum.

Thanks, corrected.

P29025, l4: mention here, that this setting optimizes SNR for high background conditions.

Good idea, done.

P29026, l4: Why do the authors chose a 20 min interval for calibration when the sonde takes only a few minutes to cover the altitude range under consideration? Why does this reduce the sampling error?

Clarified. 20 minutes seems a good compromise to us. Longer averaging periods for the RRL reduce the statistical uncertainty of the measurements but increase the sampling differences; shorter averaging results in larger statistical errors and additionally in sampling of fewer air masses which makes the comparison with the snapshot of the radiosonde even more difficult. It would be optimum, of course, to track the sonde with the RRL but such a synchronization of the lidar scanner with the sonde is not yet possible with the UHOH RRL.

P29026, l20: "the lidar temperature data" is too general here, emphasis has to be put on the 20 min average.

Clarified. We mean continuous lidar data sets for model comparisons.

P29026, l29: . . . height of maximum ++gradient++ agrees . . .

Corrected.

P29027, l14: Above the CBL. . . reformulate this phrase and say that the observed temperature fluctuations above the CBL are governed by measurement noise.

Clarified.

P29028, l5: The separation. . . this phrase is not well written.

Rewritten.

P29028, l10: There is not extrapolation "needed" since we know the ACF at lag zero. However, we want to estimate the atmospheric variability from the ACF by extrapolating the portion of non-zero lag to values of zero lag. The authors have to be more precise here, if not, the phrase starting on l12 is not comprehensible.

Rewritten as suggested.

P29028, l12: What does "at the extrapolated value" refer to here? I think one can just leave it out.

Rewritten.

P29028, l20: This looks actually more like an interpolation. Do the authors confirm that mathematically an extrapolation has been performed? and if so, From which side? Replace "the increase of the zero lag" by "the increase of the value at zero lag".

Rewritten.

P29029, l2: Why is this now called “total noise error”? Specify that the “total noise error” refers to the noise variance derived with the ACF fit.

Clarified.

P29029, l4: I guess the authors are referring to the error in temperature DUE TO photon shot noise. The error of photon shot noise does not make sense.

Rewritten.

P29029, l6: Bad use of the term “Poisson statistics”.

Rewritten.

P29029, l9: Give examples of other statistical error sources.

Done. (A few paragraphs below.)

P29029, l18ff: To what extent is this fitting process similar to the “glueing”, i.e. the determination of an offset and scaling factor a and b? The text gives the impression that the photon count signal is fitted to the analog signal, while in the standard “glueing” it is the other way around. It is not clear why the word “extrapolation” has been used.

Rewritten.

Finally, the authors must justify their approach here. Why can the noise of the analog signal be characterized by Poisson statistics, what is the physical explanation? To convince the reader further of this approach, the authors need to show (or at least verify and mention it), that this approach is in reasonable agreement with the straight forward determination of the noise, namely the standard deviation of a short de-trended portion of the analog signal. Couldn’t the difference between the statistical uncertainty in temperature derived from the ACF fit and the statistical temperature error due to shot noise be related to the fact, that the analog signal cannot be described with Poisson statistics?

We have clarified this.

P29034, l22: It is not clear from the text here which definition is used. Instead of making the reader looking it up in Lenschov et al. 2000, it should be specified here.

Clarified. We mean equation 12 just one line above.

Manuscript prepared for Atmos. Chem. Phys. Discuss.
with version 2014/09/16 7.15 Copernicus papers of the LaTeX class copernicus.cls.
Date: 9 March 2015

Profiles of second- to ~~third-order~~ forth-order moments of turbulent temperature fluctuations in the convective boundary layer: first measurements with Rotational Raman Lidar

A. Behrendt[1], **V. Wulfmeyer**[1], **E. Hammann**[1], **S. K. Muppa**[1], **and S. Pal**[2]

[1]University of Hohenheim, Institute of Physics and Meteorology, 70599 Stuttgart, Germany
[2]University of Virginia, Department of Environmental Sciences, Charlottesville, VA 22904, USA

Correspondence to: A. Behrendt (andreas.behrendt@uni-hohenheim.de)

Abstract

The rotational Raman lidar of the University of Hohenheim (UHOH) measures atmospheric temperature profiles ~~during daytime~~ with high resolution (10 s, 109 m). The data contain low noise errors even in daytime due to the use of strong UV laser light (355 nm, 10 W, 50 Hz) and a very efficient interference-filter-based polychromator. In this paper, ~~we present~~ the first profiling of the second- to forth-order moments of turbulent temperature fluctuations ~~as well as of skewness and kurtosis~~ is presented. Furthermore, skewness profiles and kurtosis profiles in the convective boundary layer (CBL) including the interfacial layer (IL) are discussed. The results demonstrate that the UHOH RRL resolves the vertical structure of these moments. The data set which is used for this case study was collected in western Germany (50°53′50.56″ N, 6°27′50.39″ E, 110 m a.s.l.) within one hour around local noon on 24 April 2013 during the Intensive Observations Period (IOP) 6 of the HD(CP)^2 Observational Prototype Experiment (HOPE), which is embedded in the German project HD(CP)^2 (High-Definition Clouds and Precipitation for advancing Climate Prediction). First, we investigated profiles of the ~~noise variance and compared it~~ total noise error of the temperature measurements and compared them with estimates of the ~~statistical~~ temperature measurement uncertainty ~~ΔT based on~~ due to shot noise derived with Poisson statistics. The ~~agreement confirms that photon count numbers obtained from extrapolated analog signal intensities provide a lower estimate of the statistical errors~~comparison confirms that the major contribution to the total statistical uncertainty of the temperature measurements originates from shot noise. The total statistical uncertainty of a 20 min temperature measurement is lower than 0.1 K up to 1050 m a.g.l. at noontime; even for single 10 s temperature profiles, it is smaller than 1 K up to ~~1000~~1020 m a.g.l.. ~~Then we confirmed by autocovariance and spectral analyses~~ Autocovariance and spectral analyzes of the atmospheric temperature fluctuations confirm that a temporal resolution of 10 s was sufficient to resolve the turbulence down to the inertial subrange. This is also indicated by the ~~profile of the~~ integral scale of the temperature fluctuations ~~, which was in the range of 40 to 120~~which had a mean value of about 80 s in the CBL ~~. Analyzing then~~ with a tendency to decrease to

smaller values towards the CBL top. Analyses of profiles of the second-, third-, and forth-order moments ~~, we found the largest values of all moments~~ show that all moments had peaks value in the IL around the mean top of the CBL which was located at 1230 m a.g.l.. The maximum of the variance profile in the IL was ~~0.40~~0.39 K^2 with ~~0.06 and 0.08~~0.07 and 0.11 K^2 for the sampling error and noise error, respectively. The third-order moment was not significantly different from zero ~~inside~~ in the CBL but showed a negative peak in the IL with a minimum of $-$~~0.72~~0.93 K^3 and values of ~~0.06 and 0.14~~0.05 and 0.16 K^3 for the sampling and noise errors, respectively. The forth-order moment and kurtosis values throughout the CBL were ~~quasi-normal.~~ not significantly different to those of a Gaussian distribution. Both showed also maxima in the IL but these were not statistically significant taking the measurement uncertainties into account. We conclude that these measurements permit the validation of large eddy simulation results and the direct investigation of turbulence parameterizations with respect to temperature.

1 Introduction

Temperature fluctuations and their vertical organization inherently govern the energy budget in the convective planetary boundary layer (CBL) by determining the vertical heat flux and modifying the interaction of vertical mean temperature gradient and turbulent transport (Wyngaard et al., 1971). Thus, the measurement of turbulent temperature fluctuations and ~~the~~ characterizations of their statistics ~~is~~ are essential for solving the turbulent energy budget closure (Stull, 1988). In-situ measurements (near the ground, on towers, or on airborne platforms) sample certain regions of the CBL within certain periods and have been used since a long time for turbulence studies. But to the best our knowledge, there are no previous observations based on a remote sensing technique suitable for this important task, i.e., resolving temperature fluctuations in high resolution and covering simultaneously the CBL up to the interfacial layer (IL). In this work, ~~we demonstrate~~ it is demonstrated that rotational Raman lidar (RRL) (Cooney, 1972; Behrendt, 2005) can fill this gap.

By simultaneous measurements of turbulence at the land surface and in the IL, the flux divergence and other key scaling variables for sensible and latent heat entrainment fluxes can be determined, which is ~~essential~~ key for the evolution of temperature and humidity in the CBL and thus for verifying turbulence parameterizations in mesoscale models (Sorbjan, 1996, 2001, 2005).

Traditionally, studies of ~~atmospheric temperature turbulence in the~~ turbulent temperature fluctuations in the atmospheric CBL were performed with in-situ instrumentation operated on tethered balloons, helicopters, and aircraft (e.g., Clarke et al., 1971; Muschinski et al., 2001); recently also with unmanned aerial vehicles (UAVs, e.g., Martin et al.,~~2001~~ 2011). However, it is not possible to obtain instantaneous profiles of turbulent fluctuations with in-situ ~~sensor~~ sensors and it is difficult to identify the exact location and characteristics of the IL. Recently, it was demonstrated the combination of remote sensing instruments (for guiding) and a UAV allows also for the study of entrainment processes at the CBL top (Martin et al., 2014). However, the UAV cannot continuously examine the processes due to its short endurance.

~~This calls~~ For studying turbulent processes and their parameterizations, however, it is essential that the turbulent transport and the temperature gradient are measured simultaneously in the same volume. Therefore, the shortcomings of in-situ observations call for new remote sensing technologies. These instruments can be operated on different platforms and can provide excellent long-term statistics, if applied from ground-based platforms. Passive remote sensing techniques, however, show difficulties in ~~achieving such coverage~~ contributing to turbulence studies because of their inherent limitation in ~~both range and time resolution as well as time dependent errors in the retrievals. E.g.~~range resolution which flattens turbulent fluctuations. Nevertheless, Kadygrov et al. (~~2011~~2003) published a study on ~~temperature turbulence~~ turbulent temperature fluctuations based on passive remote sensing techniques. The authors used a scanning microwave temperature profiler to investigate ~~boundary layer~~ thermal turbulence and ~~compared the results with~~ concluded that the spectral density of brightness temperature fluctuations at 75 m above ground indeed followed the expected $-5/3$-power law of Kolmogorov (1991)~~, however, only within the~~

lowest . Kadygrov et al. (2003) conclude that "measurements can be provided in all weather conditions, but the technique has limitations in altitude range" as their turbulence studies could reach only up to a maximum height of 200layer m.

In recent years, new insights in CBL turbulence were provided by studies based on active remote sensing with different types of radar and lidar systems. Radar wind profilers were used to study the vertical CBL wind profile and its variance (e.g., Angevine et al., 1994; Eng et al., 2000; Campistron et al., 2002). Radio-acoustic sounding systems (RASS) provide profiles of virtual temperature which can be used as scaling parameter for turbulence studies also in higher altitudes (e.g., Hermawan and Tsuda 1999; Furomoto and Tsuda 2001). But temperature and moisture fluctuations cannot be separated with RASS. Furthermore, the RASS profiles have typical resolutions of a few minutes which is too large to resolve the inertial subrange. In addition to radar, also lidar techniques have been used for turbulence studies: Elastic backscatter lidar (Pal et al., 2010, 2013), ozone differential absorption lidar (ozone DIAL) (Senff et al., 1996), Doppler lidar (e.g., Lenschow et al., 2000; Wulfmeyer and Janjic, 2005; Lenschow et O'Connor et al., 2010; Träumner et al., 2015), water vapor differential absorption lidar (WV DIAL) (e.g., Senff et al., 1994; Kiemle et al., 1997; Wulfmeyer, 1999a, b; Muppa et al., 2014), and water vapor Raman lidar (e.g., Wulfmeyer et al., 2010; Turner et al., 2014a, b) have been employed or a combination of these techniques (e.g., Giez et al., 1996; 1999; Wulfmeyer, 1999b; Kiemle et al., 2007, 2011; Behrendt et al., 2011a; Kalthoff et al., 2013). However, so far, turbulence profiling of the key CBL variable temperature profiling of turbulent temperature fluctuations with active remote sensing was missing.

In general, daytime measurements are more challenging than nighttime measurements for lidar because of the higher solar background which increases the signal noise and even prohibits measurements for most Raman lidar instruments. In order to address the measurement needs, the UHOH RRL was optimized for high temperature measurement performance in daytime in the CBL (Radlach et al., 2008). The data of the UHOH RRL have already been used for studies on the characterization of transport and optical properties of aerosol particles near their sources (Behrendt et al., 2011b; Valdebenito et al., 2011),

on the initiation of convection (Groenemeijer et al., 2009; Corsmeier et al., 2011), and on atmospheric stability indices (Behrendt et al., 2011; Corsmeier et al., 2011). Here, ~~we are applying~~ the formalism introduced by Lenschow et al. (2000) is applied for the first time to the data of an RRL to study the extension of the variable set of lidar turbulence studies within the CBL to temperature.

The measurements discussed here were carried out at local noon on 24 April 2013 during the Intensive Observations Period (IOP) 6 of the HD(CP)^2 Observational Prototype Experiment (HOPE) which is embedded in the project High-Definition Clouds and Precipitation for advancing Climate Prediction (HD(CP)^2) of the German Research Ministry. The UHOH RRL was positioned during this study at 50°53′50.56″ N, 6°27′50.39″ E, 110 m a.s.l. near the village of Hambach in western Germany where it performed measurements between 1 April and 31 May 2013.

This paper is organized as follows. In Sect. 2, the setup of the UHOH RRL is described briefly; more details can be found in (Hammann et al., 2014). The meteorological background and turbulence measurements are presented in Sect. 3. Finally, conclusions are drawn in Sect. 4.

2 Setup of the UHOH RRL

The RRL technique is based on the fact that different portions of the pure rotational Raman backscatter spectrum show different temperature dependence. By extracting signals ~~our~~ out of these two portions and forming the signal ratio, one obtains a profile which, after calibration, yields a temperature profile of the atmosphere (see, e.g., Behrendt, 2005 for details).

A scheme of the UHOH RRL during HOPE is shown in Fig. 1. Key system parameters are summarized in Table 1. As laser source, an injection-seeded frequency-tripled Nd:YAG laser (354.8 nm, 50 Hz, 10 W), model GCR 290-50 of Newport Spectra-Physics GmbH, is used. The UV laser radiation is separated from the fundamental and frequency-doubled radiation near 532 and 1064 nm, respectively, with a Pellin–Broca prism (PBP) so that only

the UV radiation is sent to the atmosphere. This improves eye-safety significantly compared to systems which use harmonic beam-splitters because definitely no potentially hazardous green laser light is present in the outgoing laser beam. But the main reason for using UV laser radiation for the transmitter of the UHOH RRL is that the backscatter cross section is proportional to the inverse wavelength to the forth power. This yields significantly stronger signals and thus lower statistical uncertainties of the measurements in the lower troposphere (see also Di Girolamo et al., 2004; Behrendt, 2005; Di Girolamo et al., 2006) when using the third harmonic instead of the second harmonic of Nd:YAG laser radiation. Behind the PBP, the laser beam is expanded 6.5-fold in order to reduce the beam divergence to $< 0.2\,\mathrm{mrad}$. The laser beam is then guided by three mirrors parallel to the optical axis of the receiving telescope (coaxial design) and reflected up into the atmosphere by two scanner mirrors inside of a so-called beam-steering unit. The same two mirrors reflect the atmospheric backscatter signals down to the receiving telescope which has a primary mirror diameter of 40 cm. The scanner allows for full hemispherical scans with a scan speed of up to $10^\circ\,\mathrm{s}^{-1}$. In the present case study, the scanner was pointing constantly in vertical direction. In the focus of the telescope, ~~an~~ a field-stop iris defines the field of view. For the data shown here, ~~we selected~~ an iris diameter of 3 mm ~~yielding~~ was selected which yielded a telescope field of view of 0.75 mrad. The light is collimated behind the iris with a convex lens and enters a polychromator which contained three channels during the discussed measurements: one channel for collecting atmospheric backscatter signals around the laser wavelength (elastic channel) and two channels for two signals from different portions of the pure rotational Raman backscatter spectrum. During the HOPE campaign, the polychromator was later extended with a water vapor Raman channel; the beamsplitter for this channel was already installed during the measurements discussed here. Within the polychromator, narrow-band multi-cavity interference filters extract in a sequence the elastic backscatter signal and the two rotational Raman signals with high efficiency. The filters are mounted at angles of incidence of about 5°. This setting allows for high reflectivity of the signals of the channels following in the chain (Behrendt and Reichardt, 2000; Behrendt et al., 2002, 2004). The filter passbands were optimized within detailed performance sim-

ulations for measurements in the CBL in daytime (Behrendt, 2005; Radlach et al., 2008; Hammann et al., 2014). The new daytime/nighttime switch for the second rotational Raman channels (Hammann et al., 2014) was set to daytime – optimizing the signal-to-noise ratio of the RR2 channel for high-background conditions. Further details on the receiver set-up and the filter passbands can be found in (Hammann et al., 2014).

3 Turbulence case study

3.1 Data set

The synoptic condition on 24 April 2013 was characterized by a large high-pressure system over central Europe. Because no clouds were forecasted for the HOPE region, this day was announced as Intensive Observation Period (IOP) 6 with the goal to study CBL development under clear-sky conditions. Indeed, undisturbed solar irradiance resulted in the development of a CBL which was not affected by clouds. A radiosonde launched at the lidar site at 11:00 UTC showed moderate westerly winds throughout the CBL and also in the lower free troposphere. The horizontal speeds were < 2 m/s near the ground increasing to about 5 m/s in the CBL between about 100 and 1000 m a.g.l.. Between 1000 and 1300 m a.g.l., the horizontal wind increased further to about 10 m/s while ranging between this value and 8 m/s in the lower free troposphere. 3-m temperatures at the lidar site increased between 9:00 to 11:00 UTC from 280 to 294 K. The sensible heat flux at noon was about 170 W/m^2 at the lidar site.

The time-height plot of the particle backscatter coefficient β_{par} (Fig. 2) between 11:00 and 12:00 UTC shows the CBL height around local noon (11:33 UTC with a maximum solar elevation of 54° on this day). β_{par} was measured with the rotational Raman lidar technique by use of a temperature-independent reference signal – (Behrendt et al., 2002). Data below 400 m were affected by incomplete geometrical overlap of the outgoing laser beam and the receiving telescope and have been excluded from this study.

~~The~~ As seen in Fig. 2, indeed no clouds were present in this period. The CBL is clearly marked by higher values of β_{par} which result from aerosol particles which are lifted up from the ground into the CBL. The instantaneous CBL height was determined with the Haar wavelet technique which detects the strongest gradient of the aerosol backscatter signal as tracer (Pal et al., 2010, 2012; Behrendt et al., 2011a) (Fig. 2). The mean of the instantaneous CBL heights z_i in the observation period was 1230 m a.g.l. This value is used in the following for the normalized height scale z/z_i. The standard deviation of the instantaneous CBL heights was 33 m; the absolute minimum and maximum were 1125 and 1323 m a.g.l., i.e., the instantaneous CBL heights were within 200 m. Besides its vertical structure, the β_{par} field in the CBL shows also a temporal trend in this case which may be explained by changing aerosol number density or size distribution in the advected air over the lidar.

The ~~UHOH RRL temperature profileof~~ temperature profile, which is the primary data product of the UHOH RRL, for the period of 11:00–11:20 UTC is shown in Fig. 3 together with z_i and the data of a local radiosonde launched at the lidar site at 11:00 UTC. Calibration of the RRL temperature data used in this study was made with these radiosonde data in the CBL between 400 and 1000 m a.g.l.; the RRL data above result from extrapolation of the calibration function. For the calibration, we used a 20 min average of the RRL data in order to reduce sampling effects between the two data sets. Longer averaging periods for the RRL reduce the statistical uncertainty of the measurements but increase the sampling differences; shorter averaging results in larger statistical errors and additionally in sampling of fewer air masses which makes the comparison with the snapshot data of the radiosonde more difficult. It would be optimum, of course, to track the sonde with the RRL but such a synchronization of the lidar scanner with the sonde is not yet possible with the UHOH RRL.

The uncertainty of the calibration depends mainly on the calibration of the radiosonde; their uncertainty is < 0.2 K according to the manufacturer (see http://www.graw.de/home/products2/radiosondes0/radiosondedfm-090/). It is noteworthy that the accuracy of the measured temperature fluctuations do not depend on the absolute

accuracy of the temperature measurements but on their relative accuracy. Even with an error of 1 K, the relative accuracy of the measured temperature fluctuations would be better than (1 K)/(250 K) = 0.4 %. For the statistical analysis of the turbulent temperature fluctuations, we ~~used then~~ then used this calibration for the one-hour RRL data set between 11:00 and 12:00 UTC. This ~~1~~1- h period seems here as a good compromise~~to us~~: for much longer periods, the CBL ~~cannot be considered as being quasi-stationary anymore~~ characteristics may change considerably while shorter periods would reduce the number of sampled thermals and thus increase the sampling errors.

The temperature profiles of RRL and radiosonde shown in Fig. 3 agree within fractions of ~~a~~one kelvin in the CBL. Larger differences occur in the IL due to the different sampling methods: the mean lidar profile shows an average over 20 min while the radiosonde data sample an instantaneous profile along the sonde's path which was determined by the drift of the sonde with the horizontal wind. In this case, the sonde needed about 5 min to reach the top of the boundary layer and was drifted by about 1.6 km away from a vertical column above the site. Depending on the part of the thermal eddies in the CBL and the IL that are sampled, the radiosonde data represent thus different CBL features and are not representative for a mean profile (Weckwerth et al., 1996) which is a crucial point to be considered when using radiosonde data for scaling of turbulent properties in the CBL. ~~Consequently, the~~ Furthermore, averaged lidar temperature data are also more representative for a certain site for model validations.

Inside the CBL, the potential temperature (derived from the RRL temperature data with the radiosonde pressure profile) is nearly constant indicating a well-mixed CBL (Fig. 3, lower panel). z_i lies approximately in the middle of the temperature inversion in the IL (Fig. 3). Figure 4 shows the temperature gradients of the radiosonde and the RRL profiles, the later for two averaging periods, namely, 11:00 to 11:20 UTC and 11:00 to 12:00 UTC. The maximum temperature gradient is ~~very similar in all these~~ in this case very similar for all three profiles, i.e., between 0.6 and 0.7 $\mathrm{K}/(100\,\mathrm{m})$~~, which, of course, is not necessarily the case for other cases~~. It is interesting to note furthermore that the height of maximum temperature gradient agrees with z_i for both RRL profiles as determined with the Haar wavelet technique~~while~~. In

contrast to this, the height of the maximum ~~gradient~~ temperature gradient in the radiosonde profile is about 60 m lower. ~~As discussed above,~~ But, as already mentioned, the radiosonde data are not representative for a mean profile.

3.2 Turbulent temperature fluctuations

For CBL turbulence analyses, the instantaneous value of temperature $T(z)$ at height z is separated in a slowly varying ~~or even constant~~ component $\overline{T(z)}$ derived from applying a linear fit to the data typically over 30 to 60 min and the temperature fluctuation $T'(z)$ according to (e.g., Wingaard, 2010)

$$T(z) = \overline{T(z)} + T'(z). \quad (1)$$

Figure 5 shows the time-height cross sections of temperature, potential temperature, and detrended temperature fluctuations $T'(z)$ in the discussed period. For detrending, ~~a linear fit~~ the same linear regression was applied to the temperature time series ~~was sufficient due to the quasi-stationary state of the CBL.~~ of all heights. Furthermore, the data set with the temperature fluctuations was gridded to exact 10-s time steps in order to ensure that all derived parameters are correct. (The vertical black lines in the lower panel of Fig. 5 are artefacts from this procedure.) One can see the positive and negative temperature fluctuations inside the CBL. In the IL, the fluctuations in the measured data become larger than in heights below. Above the CBL in the free troposphere, one finds fewer structures in the temperature fluctuations and mostly uncorrelated instrumental noise.

Lidar data contain significant stochastic instrumental noise, which has to be determined and for which has to be corrected in order to obtain the atmospheric fluctuation of a variable of interest. In general, the signal-to-noise ratio can be improved by averaging the signal in time and/or range but this in turn would of course reduce the ability to resolve turbulent structures. In principle, very high time resolution, i.e., the maximum allowed by the data acquisition system, is preferred in order to keep most frequencies of the turbulent fluctuations. But this is only possible as long as the derivation of temperature does not result in a non-linear increase of the noise errors; this noise regime should be avoided. A temporal

resolution of 10 s turned out to be a good compromise for the temporal resolution of our data as explained below.

The variance of the atmosphere $\overline{(x'_{\mathrm{a}}(z))^2}$ and the noise variance $\overline{(x'_{\mathrm{n}}(z))^2}$ of a variable x are uncorrelated. Thus, we can write (Lenschow et al., 2000)

$$\overline{(x'_{\mathrm{m}}(z))^2} = \overline{(x'_{\mathrm{a}}(z))^2} + \overline{(x'_{\mathrm{n}}(z))^2} \tag{2}$$

with $\overline{(x'_{\mathrm{m}}(z))^2}$ ~~or~~ for the measured total variance. Overbars denote here and in the following ~~mean~~ temporal averages over the analysis period. The separation of the atmospheric variance from the noise contribution ~~to the total variance~~ can be realized by different techniques. Most straightforward is the autocovariance method, which makes use of the fact that atmospheric fluctuations are correlated in time while instrumental noise fluctuations are uncorrelated. Further details were introduced by Lenschow et al. (2000) so that only a brief overview is given here. ~~By calculation of~~ The atmospheric variance can be obtained from the autocovariance function (ACF) of a variable ~~and extrapolating the function~~ by extrapolating the tails (non-zero lags) to zero lag with a power-law fit ~~, one gets the variance of the atmosphere at the extrapolated value.~~(see equation 32 of Lenschow et al., 2000). As the ACF at zero lag is the total variance, the instrumental noise variance is the difference of the two. Alternatively, one may calculate the power spectrum of the fluctuations and use Kolmogorows $-5/3$ law within the inertial subrange in order to determine the noise level ~~.~~ (e.g., O'Connor et al., 2010). We prefer the ACF method to the spectral analysis because it avoids adding additional noise and systematic effects by conversion to the frequency space.

Figure 6 shows the ACF obtained from the measured temperature fluctuations for heights between 400 and 1230 m a.g.l., i.e., 0.3 to $1.0 z_i$ for time lags from -200 to 200 s. ~~This interval was used for the extrapolation.~~ The increase of the values at zero lag with height shows mainly the increase of the statistical noise with height. Different values of the ACF close to the zero lag show differences in the atmospheric variance at different heights.

The question arises what it the most suitable number of lags for the extrapolation of the structure function to lag zero? This has been discussed in Wulfmeyer et al. (2010) and Turner et al. (2014b) but here we are providing more details. We have applied the

following procedure to the measured temperature fluctuations for the determination of the integral scale, all higher-order moments, and for the separation of noise and atmospheric variances: First of all, the profile of the integral scale is derived using a standard number of lags. Usually, we are taking 20 time lags of 10 s covering thus 200 s, as this turned out from previous measurements to be a value which is typically appropriate. The resulting integral scale is a measure of the mean size of an eddy in time. If the resulting integral scale is larger than the averaging time of the measured data, which is in this case 10 s, one can state that the most important part of the turbulent fluctuations is resolved. It can be theoretically shown that the zero crossing of the ACF appears at 2.5 times the integral scale (Wulfmeyer et al., 2015). Thus, we are choosing ≤ 2.5 times the mean value of the integral scale throughout the CBL as a reasonable number of fitlags. Please note that this refinement was not discussed in the literature before except only very recently by Turner et al. (2014b) and Wulfmeyer et al. (2015). Previously, very simple approaches were used such as just the value of the first lag as an approximation for the extrapolation to lag zero. Our approach is more appropriate and may further be refined by applying an iteration between the determination of the integral scale and the derivation of the optimal number of fitlags at each height. As the integral time scale has a mean of about 80 s in the CBL corresponding to a mean zero crossing of the ACF at 200 s, we finally decided to use 15 fitlags in this study (see Fig. 6c) which is on the safe side. We found that we can interrupt the iteration procedure in the first step because all resulting profiles are within the range of the noise error bars in this case regardless of whether we use 10, 15 or 20 fitlags. In consequence, 15 fitlags finally seemed to us as best selection. For the higher-order moments, the same number of 15 fitlags was used as for the variance but here linear extrapolations to lag zero was applied (Lenschow et al. 2000). We consider this as best approach, as the shape of the higher-order structure function is still unknown to date.

3.3 Noise errors

The resulting profiles of the ~~total~~ noise error of the temperature measurements

$$\Delta T(z) = \sqrt{\overline{(T'_{\mathrm{n}}(z))^2}} \tag{3}$$

are shown in Fig. 7 together with ~~error~~ profiles of the ~~photon shot noise~~errors due to shot-noise derived with Poisson statistics from the signal intensities (as detailed below). Both profiles are similar but it should be noted that the autocovariance technique specifies the total statistical error while ~~Poisson statistics account only for the contribution of shot noise. Thus, the results of the Poisson statistics applied to the photon-count numbers provide a lower estimate for the total errors. The comparison confirms that the photon shot noise gives the main contribution and that other statistical errorsources are comparatively small~~the shot-noise error is a part of the total statistical error.

For calculating the ~~noise error~~ shot-noise errors from the signal intensities~~with Poisson statistics~~, the following approach was made: the lidar signals are detected simultaneously in analog and in photon-counting mode. As the intensities of our rotational Raman signals are too strong, the photon-counting signals are affected by deadtime effects in lower heights than about 6 km in daytime. Correction of these deadtime effects (Behrendt et al., 2004) is possible down to about 1.5 km. As this height limit is still too high for CBL studies, ~~analog signals and not photon-counting signals~~ the analog signals have been used for the measurements of this study. In order to derive the ~~statistical uncertainty~~ shot-noise errors of the measurements with Poisson statistics, the ~~photon-counting~~ analog signals of each 10 s profile were fitted to the ~~analog~~ photon-counting signals in heights between about 1.5 and 3 km where both detection techniques were providing reliable data after deadtime correction of the photon-counting data. By ~~extrapolation~~this scaling, photon counting rates ~~were then~~ could then be attributed to the analog signal intensities in lower altitudes. These ~~extrapolated~~ attributed count rates were consequently used. The background photon-counting numbers were derived from the photon-counting signals detected from high altitudes.

The ~~statistical uncertainty of~~ ratio of the two background-corrected photon-count numbers N_{RR1} and N_{RR2} of lower and higher rotational quantum number transition channels

$$Q = \frac{N_{\mathrm{RR2}}}{N_{\mathrm{RR1}}} \tag{4}$$

is the measurement parameter which yields the atmospheric temperature profile after calibration of the system.

The shot-noise error of a signal with N photon counts according to Poisson statistics is

$$\Delta N(z) = \sqrt{N(z)}. \tag{5}$$

Error propagation ~~then yields~~ yields then for the RRL temperature data (Behrendt et al., 2002)

$$\Delta T(z) = \frac{\partial T}{\partial Q} \frac{N_{\mathrm{RR2}}(z)}{N_{\mathrm{RR1}}(z)} \sqrt{\frac{N^*_{\mathrm{RR1}}(z) + \left(\Delta \overline{B}_{\mathrm{RR1}}\right)^2}{\left(N_{\mathrm{RR1}}(z)\right)^2} + \frac{N^*_{\mathrm{RR2}}(z) + \left(\Delta \overline{B}_{\mathrm{RR2}}\right)^2}{\left(N_{\mathrm{RR2}}(z)\right)^2}}. \tag{6}$$

with $N^*_{\mathrm{RR1}}(z)$ and $N^*_{\mathrm{RR2}}(z)$ for the photon counts in the two rotational Raman channels before background correction. $N_{\mathrm{RR}i}(z) = N^*_{\mathrm{RR}i}(z) - \overline{B}_{\mathrm{RR}i}$ with $i = 1, 2$ are the signals which are corrected for background noise per range bin $\overline{B}_{\mathrm{RR}i}$. ~~The ratio of the two number of photon counts N_{RR1} and N_{RR2} of lower and higher rotational quantum number transition channels~~

$Q =$

N_{RR1} ~~is the measurement parameter which yields the atmospheric temperature profile after calibration of the system. Therefore,~~ $\partial T / \partial Q$ is provided by the temperature calibration function. As outlined already above (see section 3.1), the uncertainty of this calibration for the analysis of turbulent temperature fluctuations is negligible.

Since the background is determined over many range bins, the statistical uncertainty of the background can be neglected (Behrendt et al., 2004) so that one finally gets

$$\Delta T(z) = \frac{\partial T}{\partial Q}\frac{N_{\mathrm{RR2}}(z)}{N_{\mathrm{RR1}}(z)}\sqrt{\frac{N_{\mathrm{RR1}}(z)+\overline{B}_{\mathrm{RR1}}}{\left(N_{\mathrm{RR1}}(z)\right)^2}+\frac{N_{\mathrm{RR2}}(z)+\overline{B}_{\mathrm{RR2}}}{\left(N_{\mathrm{RR2}}(z)\right)^2}}. \tag{7}$$

~~The background counts were taken from the~~

The data shown in Fig. 7 show that the shot-noise errors calculated with Poisson statistics provide lower estimates for the total errors. But the comparison also confirms that the photon shot noise gives the major contribution (about 75 %) and that other statistical error sources (like the electric noise of the analog signals) are comparatively small. A similar result, also for analog signals which were glued to photon-counting signals~~.~~, has already been obtained before for water vapor Raman lidar by Whiteman et al. (2006).

The background-corrected rotational Raman signals scale according to

$$N_{\mathrm{RR}i}(z) \propto P\,\Delta t\,\Delta z\,\eta_{\mathrm{t}}\eta_{\mathrm{r}}\,A. \tag{8}$$

with $i = 1, 2$, laser power P, measurement time Δt, range resolution Δz, transmitter and receiver efficiency η_{t} and η_{r}, and receiving telescope area A. The background counts in each signal range bin scale in a similar way but without being influenced by power P and η_{t}, so that we get

$$\overline{B}_{\mathrm{RR}i}(z) \propto \Delta t\;\Delta z\;\eta_{\mathrm{r}}\;A. \tag{9}$$

One can see from Eqs. (7) to (9) that the statistical measurement uncertainty scales consequently with the parameters which are found in both previous equations according to

$$\Delta T \propto \frac{1}{\sqrt{\Delta t\;\Delta z\;\eta_{\mathrm{r}}\;A}}. \tag{10}$$

It is noteworthy, that increases of the laser power P and transmitter efficiency η_{t} are even more effective in reducing ΔT than increases of Δt, Δz, η_{r}, or A because the former

improve only the backscatter signals and do not increase the background simultaneously like the latter. The value of the improvement obtained from increases of P or η_t, however, depends on the intensity of the background and thus on height and background-light conditions (see also Radlach et al., 2008; Hammann et al., 2014).

The statistical uncertainties for the RRL temperature measurements at noontime shown in Fig. 7 were determined with 10 s temporal resolution and for range averaging of 109 m. The resulting error profiles for other temporal resolutions were then derived from the 10 s error profile by use of Eq. (10). The errors for other range resolutions can be easily obtained from Eq. (10) in a similar way.

The results of the error analysis show the very high performance of the UHOH RRL temperature data: with 10 s resolution, the total statistical uncertainty ΔT at noontime determined from the variance analysis of the temperature fluctuations is below 1 K up to about 1000 m a.g.l. With 1 min resolution, ΔT is below 0.4 K up to 1000 m a.g.l. and below 1 K up to ~~1530~~1510 m a.g.l. With 20 min averaging, ΔT is below 0.1 and 0.3 K up to 1050 and ~~1770~~1710 m a.g.l., respectively.

3.4 Integral scale

Figure 8 shows the ~~profiling~~ profile of the integral scale of the temperature fluctuations. It was obtained with the $2/3$-power-law fit ~~for noise correction~~ of the structure function to the ACF (Lenschow et al., 2000; Wulfmeyer et al., 2010). ~~Data around 0.9~~The integral scale is about 80 s in the mixed layer decreasing towards smaller values in the IL. At z_i, ~~i. e., that height region where the variance is close to zero and thus relative errors are very large show also relative noise errors larger than 100~~for the integral scale ~~. Consequently, these data have been excluded from the analysis. The integral scale shows values between $(40 \pm 22$~~the integral scale was (56 ± 17) s~~and (122 ± 12)s in the CBL. That the~~ . The integral scale is significantly larger than the temporal resolution of the UHOH RRL data of 10 s. This confirms that the resolution of our data is high enough to resolve the turbulent temperature fluctuations including the major part of the inertial subrange throughout the CBL. The integral time scale~~(~~, which can be related to a length scale provided that the mean horizontal

wind speed is known~~)~~ , is considered as a measure of the mean size of the turbulent eddies involved in the boundary layer mixing processes.

3.5 Temperature variance

What is to our best knowledge the first profile of the temperature variance of the atmosphere $\overline{(T'_{\mathrm{a}}(z))^2}$ measured with a lidar system is shown in Fig. 9; the profile starts at about 0.3 z_i and covers the whole CBL. ~~The variance profile was calculated with the 2/3-power-law-fit method, as discussed above. Between~~ We found that between 0.3 and 0.9 z_i, ~~the~~ i.e., the major part of the CBL, the atmospheric variance was much smaller than in the IL. Here the values ~~are~~ were only up to ~~0.058~~0.1 K^2 (at ~~982 m = 0.8z_i with 0.010 and 0.024~~1100 m = 0.9z_i with 0.01 and 0.06 K^2 for the sampling and noise error, respectively). We used the methods of (Lenschow at al., 2000) also for deriving these errors. While the noise errors denote the 1-σ statistical uncertainties of the data product due to uncorrelated noise in the time series of the input data, the sampling errors describe those uncertainties resulting from the limited number of atmospheric eddies in the analysis period. Taken the error bars into account, one finds that the apparent minimum of the temperature variance profile at ~~0.9 z_i, is not statistically significant and the one at~~ 0.6 z_i is only weakly significant. What remains is a profile with slightly increasing variance with height in the CBL and a clear maximum in the IL close to z_i. This maximum of the variance profile was ~~0.40~~0.39 K^2 with a sampling error of ~~0.06 and 0.08~~0.07 and 0.11 K^2 for the noise error (root-mean-square variability). Above, the variance decreased again. One expects such a structure for the variance profile: Except at the surface, ~~one expects that~~ the temperature variance in ~~a~~the CBL is largest in the IL since the temporal variability is driven by entrainment caused by turbulent buoyancy-driven motions acting against the temperature inversion at the top of the CBL (e.g., Deardorff, 1974; André et al., 1978; Stull, 1988; Moeng and Wyngaard, 1989).

For quantitative comparisons, often normalization of the temperature variance profile with T^* is used (Deardorf, 1970). But in the real world with its heterogeneous land-use and soil properties and thus corresponding flux variability such scaling becomes difficult. Instead

of a single scaling value, one could employ several flux stations and try to find a more representative scaling parameter by weighted averaging of the measurements made over different land-use types. But even then one expects that the scaled temperature variance profile depends on the ratio of the mean entrainment and surface flux (e.g., Moeng and Wingaard, 1989). Thus, we decided not to scale the variance profile here and leave further generalizations to future studies based on more cases.

3.6 Third-order moment and skewness

The third-order moment (TOM) of a fluctuation is a measure of the asymmetry of the distribution. The skewness S is the TOM normalized by the variance to a dimensionless parameter defined for temperature as

$$S(z) = \frac{\overline{(T'(z))^3}}{\left(\overline{(T'(z))^2}\right)^{3/2}}. \tag{11}$$

The normal distribution (Gaussian curve) has zero TOM and S. Positive values for TOM and S show a right-skewed distribution where the mode is smaller than the mean. If the mode is larger than the mean, TOM and S become negative (left-skewed distribution).

TOM and S profiles for the atmospheric temperature fluctuations of our case were derived with the technique of (Lenschow et al., 2000) as explained in section 3.2.. The results are shown in Fig. 10. Up to about 0.9 z_i, the TOM was not different to zero (taking the 1-σ statistical uncertainties into account). In the IL, i.e., between 0.9 and 1.1 z_i, a negative peak is found with values down to ~~-0.72~~0.93 K^3 with ~~0.06 and 0.14~~0.05 and 0.16 K^3 for the sampling and noise errors, respectively. The skewness profile shows the same characteristics. Only data around ~~0.9~~ 0.6 z_i had to be omitted from the ~~analysis because the variance profile becomes~~ skewness profile because the measured variance values are close to zero here and thus division by these values ~~yielded~~ yields too large relative errors. At z_i, we found a skewness of ~~-3.2 with 0.9 and 1.3~~ 4.1 with 1.1 and 1.9 for the sampling and noise errors, respectively.

TOM and S profiles reveal interesting characteristics of the thermal plumes which were present in the CBL in this case. ~~We can conclude that the turbulent temperaturefluctuations were not significantly skewed in the CBL; negative and positive fluctuations were symmetric. The negative minimum~~ As rising plumes of warmer air are typically narrow and surrounded by larger areas of air close to the average temperature, one expects slightly positive temperature skewness in the major part of the CBL. E.g., Mironov et al. (1999) show values between 0 and 2 (see their figure 1b); they did not show negative values which would indicate narrow cold plumes. In the CBL up to about 0.9 z_i, the measured values in our case agree with these data taking the uncertainties into account.

The negative minima of TOM and S in the IL ~~shows~~ above show a clear difference between the IL and the CBL below. Between 0.9 and 1.1 z_i, negative and positive fluctuations were not symmetric but fewer very cold fluctuations were balanced by many warm fluctuations with less difference to the mean.

Because turbulent mixing occurs in the IL in a region of positive vertical temperature gradient~~in the IL~~, the air present in the free troposphere is warmer than the air in the CBL below. Consequently, the negative peak indicates that the cold overshooting updrafts in the IL were narrower in time than the downdrafts of warmer air.

Similar characteristics of the temperature TOM and skewness profiles in the ~~CBL~~ IL were discussed, e.g., by Mironov et al. (1999), Canuto et al. (2001), and Cheng et al. (2005) who compare experimental data (tank, wind tunnel, airborne in-situ), LES data, and analytical expressions. Now, more comparisons can be performed between real atmospheric measurements and models.

Interestingly, an inverse structure of the TOM profile is found with respect to humidity fluctuations (Wulfmeyer 1999b, Wulfmeyer et al. 2010, Turner et al. 2014b). Combining these results, it should be possible to perform very detailed comparisons with LES and to refine turbulence parameterizations. This concerns particularly the TKE 3.0 order schemes that are using the closure of the variance budget for determining the turbulent exchange coefficients.

3.7 Forth-order moment and kurtosis

~~Forth-order~~ The forth-order moment (FOM) is a measure of the steepness at the sides of the distribution and the corresponding flatness of the peak. The kurtosis is the FOM normalized by the variance to a dimensionless parameter according to

$$\text{Kurtosis}(z) = \frac{\overline{(T'(z))^4}}{\left(\overline{(T'(z))^2}\right)^2}. \quad (12)$$

With this definition, the normal distribution (Gauss curve) has a kurtosis of 3. ~~(We follow the same definition as~~ Equation 12 is also used by Lenschow et al. (2000)~~for kurtosis ;~~ we follow this definition here. Please note that sometimes kurtosis is defined differently including a subtraction of 3 which results then in a kurtosis of 0 for the normal distribution.~~)~~ ; but mostly Kurtosis - 3 is called "excess kurtosis".

Figure 11 shows FOM and kurtosis profiles of the measured temperature fluctuations of our case. For both FOM and kurtosis, the noise errors of the data are quite large; the importance of an error analysis becomes once more obvious. Throughout the CBL, no significant differences to the normal distribution are found. While the values for the FOM are close to zero in the CBL ($< 0.5\,\mathrm{K}^4$ up to 0.9 z_i), they appear larger in the IL, but the noise error does not allow for determining exact values, zero is still within the 1-σ noise error bars. At z_i, FOM was ~~2.7~~3.0 K^4 with ~~0.2 and 3.7~~0.1 and 4.2 K^4 for the sampling and noise errors, respectively. The kurtosis at z_i was ~~20 with 7 and 28~~ 23 with 8 and 35 for the sampling and noise errors, respectively. We conclude that the distribution of atmospheric temperature fluctuations was not significantly different to a Gaussian distribution (quasi-normal) regarding its forth-order moment and kurtosis in our case.

Even if the data is here too noisy to identify non-zero FOM or kurtosis in the IL, it is interesting to note that higher values of kurtosis in the IL would reflect a situation for which a large fraction of the temperature fluctuations occurring in this region would exist due to infrequent very large deviations in temperature; the related most vigorous thermals would then be capable to yield quite extreme temperature fluctuations while mixing intensively

in the IL with the air of the lower free troposphere. In contrast to this, the temperature fluctuations would be more moderate (Gaussian) in the CBL below.

4 Conclusions

We have shown that rotational Raman lidar ~~offers~~ provides a remote sensing technique for the analysis of the turbulent temperature fluctuations within the well-developed CBL during noontime – even though the background light conditions at noon are least favorable for ~~measurements with rotational Raman lidar. We can state that the~~ the measurements. The required high temporal and spatial resolution combined with low-enough statistical noise of the measured data is reached by the UHOH RRL what is to our knowledge for the first time. The data can thus be evaluated during the all time periods of the day for studying the structure of the atmospheric boundary layer – of course also at night.

~~We have analyzed a~~A case of the HOPE campaign was analyzed. The data were collected between 11:00 and 12:00 UTC on IOP 6, 24 April 2013, i.e., exactly around local noon (11:33 UTC). The UHOH RRL was located near the village of Hambach in western Germany (50°53′50.56″ N, 6°27′50.39″ E, 110 m a.s.l.).

A profile of the noise variance was used to estimate the statistical uncertainty ΔT of the temperature data with a ~~2/3 power law~~ structure function fit to the autocovariance function. A comparison with a ΔT profile derived with Poisson statistics demonstrated that the statistical error is mainly due to shot noise. The Haar wavelet technique was applied to 10 s profiles of β_{par} and provided the mean CBL height over the observation period of $z_i = 1230$ m a.g.l. This value ~~is~~ was used for normalizing the height scale.

~~The results of this study give further information on turbulent temperature fluctuations and their statistics in the CBL and within the IL. The integral scale profile shows values between (40 ± 22) s and (122 ± 12) s~~ The integral scale had a mean of about 80 s in the CBL ~~. Thus, we can confirm~~ confirming that the temporal resolution of the RRL data of 10 s was ~~sufficiently high~~ sufficient for resolving the major part of turbulence down to the inertial subrange.

The results of this study give further information on turbulent temperature fluctuations and their statistics in the CBL and within the IL.

The atmospheric variance profile showed clearly the largest values close to z_i. A maximum of the variance of the atmospheric temperature fluctuations was found in the IL: ~~0.40~~0.39 K^2 with a sampling and noise error of ~~0.06 and 0.08~~0.07 and 0.11 K^2, respectively. ~~Subsequently, we also derived~~

Subsequently, also profiles of the third- and forth-order moments ~~.~~ were derived:

TOM and skewness were not significantly different to zero within the CBL up to about 0.9 z_i. In the IL between 0.9 and 1.1 z_i, a negative minimum was found with values down to $-$~~0.72~~0.93 K^3 with ~~0.06 and 0.14~~0.05 and 0.16 K^3 for the sampling and noise errors, respectively. Skewness at z_i was $-$~~3.2 and with 0.9 and 1.3~~ 4.1 and with 1.1 and 1.9 for the sampling and noise errors, respectively. We conclude that the turbulent temperature fluctuations were not significantly skewed in the CBL. In contrast to this, the atmospheric temperature fluctuations in the IL were clearly skewed to the left (negative skewness). This finding is related to narrower cold overshooting updrafts and broader downward mixing of warmer air from the free troposphere in the IL.

Throughout the CBL, no significant differences to the normal distribution were found for FOM and the kurtosis. For all moments but especially the FOM, the importance of an error analysis became once more obvious.

A quasi-normal FOM even when TOM is non-zero, agrees with the hypothesis of Millionshchikov (1941) which forms the basis for a large number of closure models (see Gryanik et al., 2005 for an overview). However, some recent theoretical studies, measurement data, and LES data suggest that this hypothesis would not be valid for temperature in the CBL (see also see Gryanik et al., 2005 for an overview). Gryanik and Hartmann (2005) suggested furthermore a parametrization between the FOM, skewness and variance of turbulent temperature fluctuations which can be tested as soon as a larger number of measurement cases on turbulent temperature fluctuations with rotational Raman lidar has become available.

It is planned to extend the investigation of CBL characteristics in future studies also by combining the UHOH RRL data with humidity and wind observations from water vapor DIAL (Muppa et al., 2014~~; Spth et al., 2014~~) and Doppler lidar. Furthermore, also the scanning capability of the UHOH RRL will be used in future to collect data closer to the ground and even the surface layer (Behrendt et al., 2012) in order to investigate heterogeneities over different terrain.

The combination of different turbulent parameters measured by lidar – preferably, at the same atmospheric coordinates simultaneously – promises to provide further understanding on the important processes taking place in the CBL including the IL. For instance, till date, the key physical processes governing the IL and their relationships with other CBL properties remain unfortunately only poorly understood: they are oversimplified in empirical studies and poorly represented in the models. In consequence, more data should be evaluated to get the statistics of ~~temperature turbulence~~ the turbulent temperature fluctuations under a variety of atmospheric conditions. We believe that ~~temperature turbulence profiling~~ corresponding measurements with RRL will contribute significantly to better understanding of boundary layer meteorology in the future – not only in daytime but also at night so that the entire diurnal cycle is covered and the characteristics of ~~temperature turbulence~~ turbulent temperature fluctuations in different stability regimes can be observed.

References

André, J. C., De Moor, G., Lacarrère, P., Therry, G., and Du Vachat, R.: Modeling the 24-hour evolution of the mean and turbulent structures of the planetary boundary layer, J. Atmos. Sci., 35, 1861–1883, 1978.

Angevine, W. M., Doviak, R. J., and Sorbjan, Z. S.: Remote Sensing of Vertical Velocity Variance and Surface Heat Flux in a Convective Boundary Layer, J. Appl. Meteorol. 33, 977983, 1994.

Behrendt, A.: Temperature measurements with lidar, in: Lidar: Range-Resolved Optical Remote Sensing of the Atmosphere, edited by: Weitkamp, C., Springer, New York, 273–305, 2005.

Behrendt, A. and Reichardt, J.: Atmospheric temperature profiling in the presence of clouds with a pure rotational Raman lidar by use of an interference-filter-based polychromator, Appl. Optics, 39, 1372–1378, 2000.

Behrendt, A., Nakamura, T., Onishi, M., Baumgart, R., and Tsuda, T.: Combined Raman lidar for the measurement of atmospheric temperature, water vapor, particle extinction coefficient, and particle backscatter coefficient, Appl. Optics, 41, 7657–7666, 2002.

Behrendt, A., Nakamura, T., and Tsuda, T.: Combined temperature lidar for measurements in the troposphere, stratosphere, and mesosphere, Appl. Optics, 43, 2930–2939, 2004.

Behrendt, A., Wulfmeyer, V., Riede, A., Wagner, G., Pal, S., Bauer, H., Radlach, M., and Späth, F.: 3-Dimensional observations of atmospheric humidity with a scanning differential absorption lidar. In Richard H. Picard, Klaus Schäfer, Adolfo Comeron et al. (Eds.), Remote Sensing of Clouds and the Atmosphere XIV, SPIE Conference Proceeding Vol. 7475, ISBN: 9780819477804, 2009, Art. No. 74750L, DOI:10.1117/12.835143, 2009.

Behrendt, A., Pal, S., Aoshima, F., Bender, M., Blyth, A., Corsmeier, U., Cuesta, J., Dick, G., Dorninger, M., Flamant, C., Di Girolamo, P., Gorgas, T., Huang, Y., Kalthoff, N., Khodayar, S., Mannstein, H., Träumner, K., Wieser, A., and Wulfmeyer, V.: Observation of convection initiation processes with a suite of state-of-the-art research instruments during COPS IOP8b, Q. J. Roy. Meteor. Soc., 137, 81–100, doi:10.1002/qj.758, 2011a.

Behrendt, A., Pal, S., Wulfmeyer, V., Valdebenito B., Á. M., and Lammel, G.: A novel approach for the char-acterisation of transport and optical properties of aerosol particles near sources, Part I: measurement of particle backscatter coefficient maps with a scanning UV lidar, Atmos. Environ., 45, 2795–2802, doi:10.1016/j.atmosenv.2011.02.061, 2011b.

Behrendt, A., Hammann, E., Späth, F., Riede, A., Metzendorf, S., and Wulfmeyer, V.: Revealing surface layer heterogeneities wit scanning water vapor DIAL and scanning rotational Raman lidar, in: Reviewed and Revised Papers Presented at the 26th International Laser Radar Conference (ILRC 2012), 25–29 June 2012, Porto Heli, Greece, edited by: Papayannis, A., Balis, D., and Amiridis, V., paper S7P-17, 913–916, 2012.

Campistron, B., Bernard, S., Bch, B., Ardhuin-Girard, F., Dessens, J., Dupont, E., Carissimo, B.: Turbulent Dissipation Rate In The Boundary Layer Via Uhf Wind Profiler Doppler Spectral Width Measurements. Bound.-Lay. Meteorol., 103, 361–389, 2002.

Canuto, V. M., Chang, Y., and Howard, A.: New third-order moments for the convective boundary layer, J. Atmos. Sci., 58, 1169–1172, 2001.

Cheng, Y., Canuto, V. M., and Howard, A. M.: Nonlocal convective PBL Model based on new third- and forth-order moments, J. Atmos. Sci., 62, 2189–2204, 2005.

Clarke, R. H., Dyer, A. J., Brook, R. R., Reid, D. G., and Troup, A. J.: The Wangara experiment: Boundary layer data. Tech. Paper No. 19, CSIRO, Division of Meteorological Physics, Aspendale, Australia, 362 pp., 1971.

Cooney, J.: Measurement of atmospheric temperature profiles by Raman backscatter, J. Appl. Meteorol., 11, 108–112, 1972.

Corsmeier, U., Kalthoff, N., Barthlott, Ch., Behrendt, A., Di Girolamo, P., Dorninger, M., Aoshima, F., Handwerker, J., Kottmeier, C., Mahlke, H., Mobbs, S., Vaughan, G., Wickert, J., and Wulfmeyer, V.: Driving processes for deep convection over complex terrain: a multiscale analysis of observations from COPS-IOP 9c, Q. J. Roy. Meteor. Soc., 137, 137–155, doi:10.1002/qj.754, 2011.

Deardorff, J. W.: Convective velocity and temperature scales for the unstable planetary boundary layer and for Rayleigh convection, J. Atmos. Sci., 27, 1211 –1213, 1970.

Deardorff, J. W.: Three-dimensional numerical study of turbulence in an entraining mixed layer, Bound.-Lay. Meteorol., 7, 199–226, 1974.

Di Girolamo, P., Marchese, R., Whiteman, D. N., and Demoz, B.: Rotational Raman lidar measurements of atmospheric temperature in the UV, Geophys. Res. Lett., 31, L01106, doi:10.1029/2003GL018342, 2004.

Di Girolamo, P., Behrendt, A., and Wulfmeyer, V.: Spaceborne profiling of atmospheric temperature and particle extinction with pure rotational Raman lidar and of relative humidity in combination with differential absorption lidar: performance simulations, Appl. Optics, 45, 2474–2494, 2006.

Eng, K., Coulter, R., and Brutsaert, W.: Vertical Velocity Variance in the Mixed Layer from Radar Wind Profilers. J. Hydrol. Eng., 8, 301-307, 2003.

Giez, A., Ehret, G., Schwiesow, R. L., Davis, K. J., and Lenschow, D. H.: Water vapor flux measurements from ground-based vertically pointed water vapor differential absorption and Doppler lidars, J. Atmos. Ocean. Tech., 16, 237–250, 1999.

Groenemeijer, P., Barthlott, C., Behrendt, A., Corsmeier, U., Handwerker, J., Kohler, M., Kottmeier, C., Mahlke, H., Pal, S., Radlach, M., Trentmann, J., Wieser, A., and Wulfmeyer, V.: Multi-sensor measurements of a convective storm cluster over a low mountain range: adaptive observations during PRINCE, Mon. Weather Rev., 137, 585–602, doi:10.1175/2008MWR2562.1, 2009.

Gryanik, V.M., and Hartmann, J.: A turbulence closure for the convective boundary layer based on a two-scale mass-flux approach. J. Atmos. Sci., 59, 27292744, 2002.

Gryanik, V. M., Hartmann, J., Raasch, S., and Schröter, M.: A refinement of the Millionshchikov Quasi-Normality Hypothesis for convective boundary layer turbulence, J. Atmos. Sci., 62, 2632–2638, 2005.

Hammann, E., Behrendt, A., Le Mounier, F., and Wulfmeyer, V.: Temperature profiling of the atmospheric boundary layer with Rotational Raman lidar during the HD(CP)2 observational prototype experiment, Atmos. Chem. Phys., ~~submitted, 2014.~~ accepted, 2015.

Hermawan, E., and Tsuda, T.: Estimation of turbulence energy dissipation rate and vertical eddy diffusivity with the MU radar RASS, Journal of Atmospheric and Solar-Terrestrial Physics, 61, 1123-1130, doi:10.1016/S1364-6826(99)00075-9, 1999.

Kadygrov, E. N., Shur, G. N., and Viazankin, A. S.: Investigation of atmospheric boundary layer temperature, turbulence, and wind parameters on the basis of passive microwave remote sensing, Radio Sci., 38, 8048, doi:10.1029/2002RS002647, 2003.

Kalthoff, N., Träumner, K., Adler, B., Späth, S., Behrendt, A., Wieser, A., Handwerker, J., Madonna, F., and Wulfmeyer, V.: Dry and moist convection in the boundary layer over the Black Forest – a combined analysis of in situ and remote sensing data, Meteorol. Z., 22, 445–461, doi:10.1127/0941-2948/2013/0417, 2013.

Kiemle, C., Ehret, G., Giez, A., Davis, K. J., Lenschow, D. H., and Oncley, S. P.: Estimation of boundary layer humidity fluxes and statistics from airborne differential absorption lidar (DIAL), J. Geophys Res., 102, 29189–29203, 1997.

Kiemle, C., Brewer, W. A., Ehret, G., Hardesty, R. M., Fix, A., Senff, C., Wirth, M., Poberaj, G., and LeMone, M. A.: Latent heat flux profiles from collocated airborne water vapor and wind lidars during IHOP 2002, J. Atmos. Ocean. Tech., 24, 627–639, 2007.

Kiemle, C., Wirth, M., Fix, A., Rahm, S., Corsmeier, U., and Di Girolamo, P.: Latent heat fluxes over complex terrain from airborne water vapour and wind lidars, Q. J. Roy. Meteor. Soc., 137, 190–203, 2011.

Kolmogorov, A. N.: The Local Structure of Turbulence in Incompressible Viscous Fluid for Very Large Reynolds Numbers, Proc. R. Soc. Lond., A 434, 1890, 9–13, doi:10.1098/rspa.1991.0075, 1991.

Lenschow, D. H., Wulfmeyer, V., and Senff, C.: Measuring second through fourth-order moments in noisy data, J. Atmos. Ocean. Tech., 17, 1330–1347, 2000.

Lenschow, D. H., Lothon, M., Mayor, S. D., Sullivan, P. P., and Caunt., G.: A comparison of higher-order vertical velocity statistics in the convective boundary layer from lidar with in-situ measurements and large-eddy simulations, Bound.-Lay. Meteorol., 143, 107–123, 2012.

Martin, S., Bange, J., and Beyrich, F.: Meteorological profiling of the lower troposphere using the research UAV "M^{2}AV Carolo", Atmos. Meas. Tech., 4, 705–716, doi:10.5194/amt-4-705-2011, 2011.

Martin, S., Beyrich, F., and Bange, J.: Observing Entrainment Processes Using a Small Unmanned Aerial Vehicle: A Feasibility Study, Bound.-Lay. Meteorol., 150, 449-467, 2014.

Millionshchikov, M. D.: On the Theory of Homogeneous Isotropic Turbulence, Dokl. Akad. Nauk SSSR, 32, 611–614, 1941.

Mironov, D. V., Gryanik, M., Lykossov, V. N., and Zilitinkevich, S. S.: Comments on "A new second-order turbulence closure scheme for the planetary boundary layer", J. Atmos. Sci., 56, 3478–3481, 1999.

Moeng, C.-H. and Wyngaard, J. C.: Evaluation of turbulent transport and dissipation closures in second-order modelling, J. Atmos. Sci., 46, 2311–2330, 1989.

Muppa, S. K., Behrendt, A., Späth, F., Wulfmeyer, V., Metzendorf, S., and Riede, A.: Turbulent humidity fluctuations in the convective boundary layer: ~~case~~ Case studies using DIAL measurements, ~~Atmos.Chem. Phys.Discuss., in preparation~~Bound.-Lay. Meteorol., submitted, 2014.

Muschinski, A., Frehlich, R., Jensen, M., Hugo, R., Eaton, F., and Balsley, B.: Fine-scale measurements of turbulence in the lower troposphere: an intercomparison between a kite- and balloon-borne, and a helicopter-borne measurement system, Bound.-Lay. Meteorol., 98, 219–250, 2001.

OConnor, E., Illingworth, A., Brooks, I., Westbrook, M., Christopher, D., Hogan, R., Davies, F., and Brooks, B.: A Method for Estimating the Turbulent Kinetic Energy Dissipation Rate from a Vertically Pointing Doppler Lidar, and Independent Evaluation from Balloon-Borne In Situ Measurements, J. Atmos. Ocean. Tech., 27, 16521664, doi:10.1175/2010JTECHA1455.1, 2010.

Pal, S., Behrendt, A., and Wulfmeyer, V.: Elastic-backscatter-lidar-based characterization of the convective boundary layer and investigation of related statistics, Ann. Geophys., 28, 825–847, doi:10.5194/angeo-28-825-2010, 2010.

Pal, S., Xueref-Remy, I., Ammoura, L., Chazette, P., Gibert, F., Royer, P., Dieudonné, E., Dupont, J. C., Haeffelin, M., Lac, C., Lopez, M., Morille, Y., and Ravetta, F.: Spatio-temporal variability of the atmospheric boundary layer depth over the Paris agglomeration: an assessment of the impact of the urban heat island intensity, Atmos. Environ., 63, 261–275, 2012.

Pal, S., Haeffelin, M, and Batchvarova, E. Exploring a geophysical process-based attribution technique for the determination of the atmospheric boundary layer depth using aerosol lidar and near-surface meteorological measurements, J. Geophys. Res.-Atmos., 118, 1–19, doi:10.1002/jgrd.50710, 2013.

Radlach, M., Behrendt, A., and Wulfmeyer, V.: Scanning rotational Raman lidar at 355 nm for the measurement of tropospheric temperature fields, Atmos. Chem. Phys., 8, 159–169, doi:10.5194/acp-8-159-2008, 2008.

Senff, C. J., Bösenberg, J., and Peters, G.: Measurement of water vapor flux profiles in the convective boundary layer with lidar and Radar-RASS, J. Atmos. Ocean. Tech., 11, 85–93, 1994.

Senff, C. J., Bösenberg, J., Peters, G., and Schaberl, T.: Remote sensing of turbulent ozone fluxes and the ozone budget in the convective boundary layer with DIAL and radar-RASS: a case study, Contrib. Atmos. Phys., 69, 161–176, 1996.

Sorbjan, Z.: Effects caused by varying the strength of the capping inversion based on a large eddy simulation model of the shear-free convective boundary layer, J. Atmos. Sci., 53, 2015–2024, 1996.

Sorbjan, Z: An evaluation of local similarity on the top of the mixed layer based on large-eddy simulations, Bound.-Lay. Meteorol., 101, 183–207, 2001.

Sorbjan, Z.: Statistics of scalar fields in the atmospheric boundary layer based on large-eddy simulations, Part I: free convection, Bound.-Lay. Meteorol., 116, 467–486, 2005.

~~Spth, F., Behrendt, A., Muppa, S. K., Metzendorf, S., Riede, A., and Wulfmeyer, V.: High-resolution atmospheric water vapor measurements with a scanning differential absorption lidar, Atmos. Chem. Phys., submitted, 2014.~~

Stull, R. B.: An Introduction to Boundary Layer Meteorology, Springer, Heidelberg, New York, 688 pp., 1988.

Turner, D. D., Ferrare, R. A., Wulfmeyer, V., and Scarino, A. J.: Aircraft evaluation of ground-Based Raman lidar water vapor turbulence profiles in convective mixed layers, J. Atmos. Ocean. Tech., 31, 1078–1088, doi:10.1175/JTECH-D-13-00075.1, 2014a.

Turner, D. D., Wulfmeyer, V., Berg, L. K., and Schween, J. H.: Water vapor turbulence profiles in stationary continental convective mixed layers, J. Geophys. Res., 119, 1–15, doi:10.1002/2014JD022202, 2014b.

Träumner, K., Damian, Th., Stawiarski, Ch., Wieser, A.: Turbulent Structures and Coherence in the Atmospheric Surface Layer. Boundary-Layer Meteorol., 154, 1-25, doi:10.1007/s10546-014-9967-6, 2015.

Valdebenito, A. M., Pal, S., Lammel, G., Behrendt, A., and Wulfmeyer, V.: A novel approach for the characterisation of transport and optical properties of aerosol particles near sources: microphysics-chemistry-transport model development and application, Atmos. Environ., 45, 2981–2990, doi:10.1016/j.atmosenv.2010.09.004, 2011.

Wagner, G., Wulfmeyer, V., Späth, F., Behrendt, A., and Schiller, M.: Performance and specifications of a pulsed high-power single-frequency Ti:Sapphire laser for water-vapor differential absorption lidar. Appl. Opt. 52, 2454-2469, DOI:10.1364/AO.52.002454, 2013.

Weckwerth, T. M., Wilson, J. W., and Wakimoto, R. M.: Thermodynamic variability within the convective boundary layer due to horizontal convective rolls, Mon. Weather Rev., 124, 769–784, 1996.

Whiteman, D. N.,Demoz,B., Di Girolamo, P.,Comer, J., Veselovskii, I., Evans, K., Wang, Z., Sabatino, D., Schwemmer, G., Gentry, B., Lin, R-F., Behrendt, A., Wulfmeyer, V., Browell, E., Ferrare, R., Ismail, S. and Wang, J.: Raman Lidar Measurements during the International H2O Project. Part II: Case Studies, J. Atmos. Oceanic Technol., 23, 170-183, 2006.

Wulfmeyer, V.: Investigations of humidity skewness and variance profiles in the convective boundary layer and comparison of the latter with large eddy simulation results, J. Atmos. Sci., 56, 1077–1087, 1999a.

Wulfmeyer, V.: Investigation of turbulent processes in the lower troposphere with water-vapor DIAL and radar-RASS, J. Atmos. Sci., 56, 1055–1076, 1999b.

Wulfmeyer, V. and Janjic, T.: 24-h observations of the marine boundary layer using ship-borne NOAA high-resolution Doppler lidar, J. Appl. Meteorol., 44, 1723–1744, 2005.

Wulfmeyer, V., Pal, S., Turner, D. D., and Wagner, E.: Can water vapour ~~raman~~ Raman lidar resolve profiles of turbulent variables in the convective boundary layer?, Bound.-Lay. Meteorol., 136, 253–284, doi:10.1007/s10546-010-9494-z, 2010.

Wulfmeyer, V., Behrendt, A., Sorbian, Z., Turner, D. D., and Hardesty, R. M.: Determination of Convective Boundary Layer Entrainment Fluxes, Dissipation Rates, and the Molecular Destruction of Variances: Theoretical Description and a Strategy for its Confirmation with a Novel Lidar System Synergy, J. Atmos. Sci., submitted, 2015.

Wyngaard, J. C. and Cote, O. R.: The budgets of turbulent kinetic energy and temperature variance in the atmospheric surface layer, J. Atmos. Sci., 28, 190–201, 1971.

Wyngaard, J. C.: Turbulence in the Atmosphere, Cambridge University Press, 2010.

Table 1. Overview of key parameters of the Rotational Raman Lidar of University of Hohenheim (UHOH RRL) during the measurements discussed here.

Transmitter	Flash-lamp-pumped injection-seeded frequency-tripled Nd:YAG laser Pulse energy: ~ 200 mJ at 354.8 nm Repetition rate: 50 Hz Pulse duration: ~ 5 ns
Receiver	Diameter of primary mirror: 40 cm Focal length: 4 m Field of view: 0.75 mrad (selectable)
Scanner	Manufactured by the NCAR, Boulder, CO, USA Mirror coating: Protected aluminum Scan speed: Up to $10^\circ\,s^{-1}$
Detectors	Photomultiplier Tubes, Hamamatsu R7400-U02 (Elastic), R1924P (RR1+2)
Data Acquisition System	3-channel transient-recorder, LICEL GmbH, Germany
Range resolution	3.75 m in analog mode up to 30 km range 3.75 m in photon-counting mode up to 30 km range 37.5 m in photon-counting mode up to 75 km range

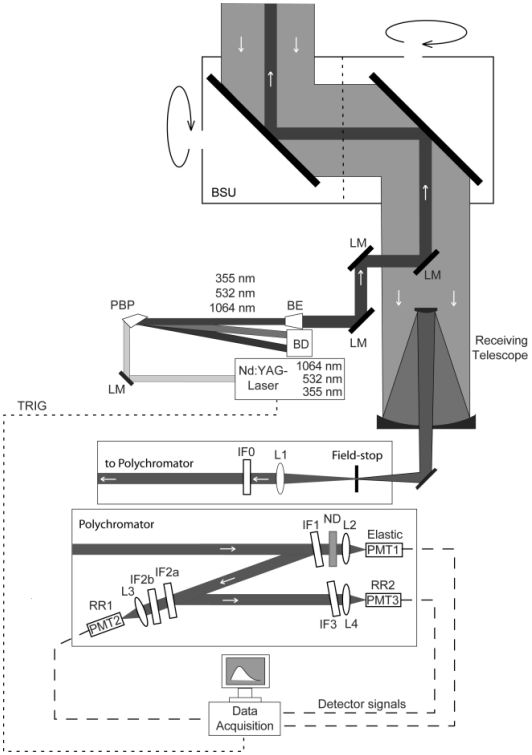

Figure 1. Scheme of the UHOH RRL. The beam-steering unit (BSU) consists of two plane mirrors which scan the laser beam and receiving telescope field-of-view. LM: Laser mirror; PBP: ~~Pelin–Broca~~ Pellin–Broca prism; BE: Beam expander; BD: Beam dump; L1 to ~~L6~~L4: lenses; IF0 to IF3: Interference filters; ~~OF: Optical Fiber;~~ PMT1 to PMT3: Photomultiplier Tubes; RR1 and RR2: Rotational Raman channel 1 and 2, respectively. The beamsplitter for the water vapor Raman channel between L1 and IF0 has been omitted for clarity here.

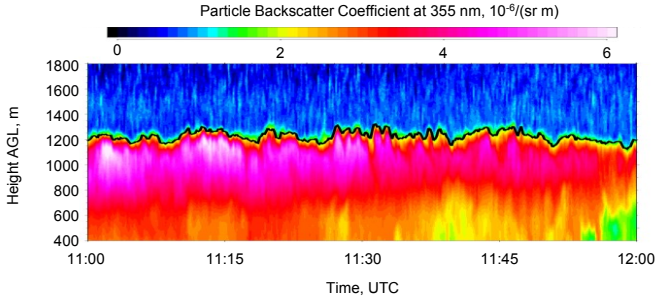

Figure 2. Time-height cross section of particle backscatter coefficient β_{par} at 354.8 nm measured with the UHOH RRL on 24 April 2013 between 11:00 and 12:00 UTC. The temporal and spatial resolution of the data is $\Delta t = 10$ s and $\Delta z = 3.75$ m with a gliding average of 109 m. The instantaneous CBL heights determined with the Haar-wavelet analysis of β_{par} profiles are marked. a.g.l.: above ground level.

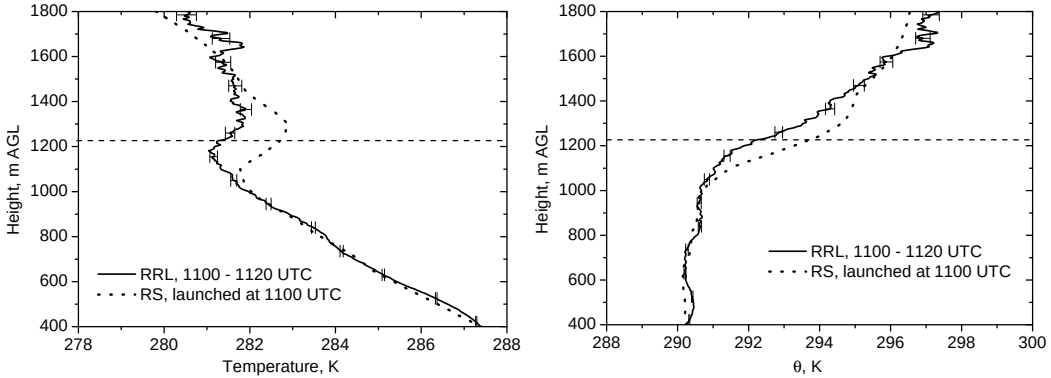

Figure 3. Upper panel: average temperature profile measured with the UHOH RRL on 24 April 2013 between 11:00 and 11:20 UTC and temperature profiles measured with a local radiosonde launched at the lidar site at 11:00 UTC. Lower panel: same but potential temperature profiles. The dashed line shows z_i for comparison. Error bars show the uncertainties derived with Poisson statistics from the intensities of the rotational Raman signals.

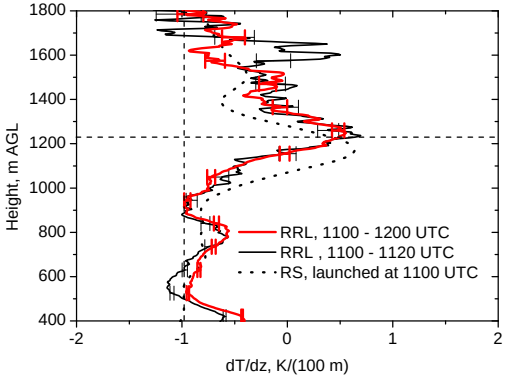

Figure 4. Average temperature gradients measured with the UHOH RRL on 24 April 2013 between 11:00 and 11:20 UTC, between 11:00 and 12:00 UTC and temperature gradient measured with a local radiosondes launched at the lidar site at 11:00 UTC. The horizontal dashed line shows z_i, the mean CBL top height for the period between 11:00 and 12:00 UTC, which agrees with the maximum temperature gradients of both RRL profiles. The vertical dashed line shows the dry-adiabatic temperature gradient. Error bars show the uncertainties derived with Poisson statistics from the intensities of the rotational Raman signals.

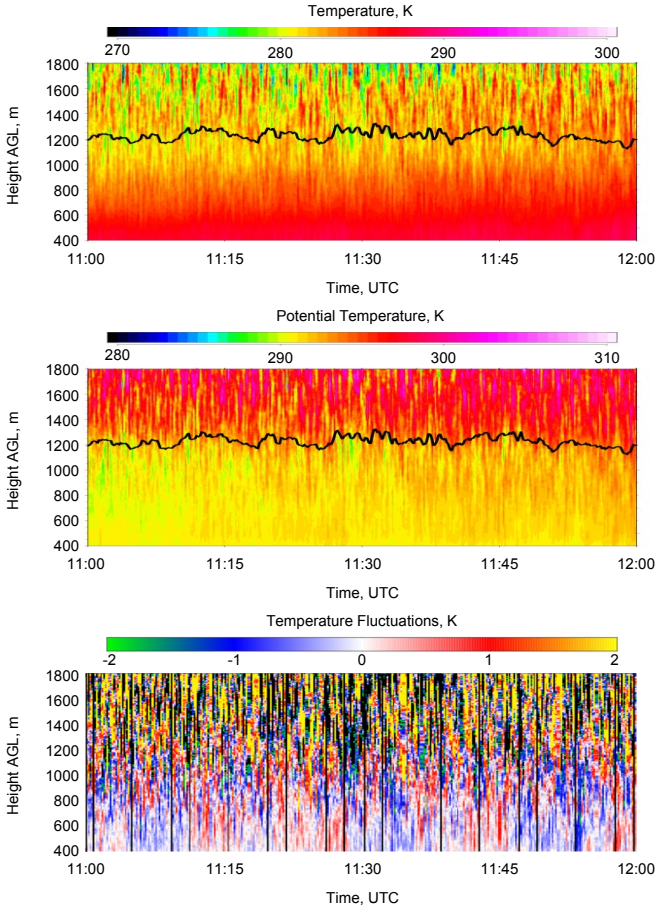
Temperature, K
270
280
290
300
Height AGL, m
1800
1600
1400
1200
1000
800
600
400
11:00
11:15
11:30
11:45
12:00
Time, UTC
Potential Temperature, K
280
290
300
310
Height AGL, m
1800
1600
1400
1200
1000
800
600
400
11:00
11:15
11:30
11:45
12:00
Time, UTC
Temperature Fluctuations, K
-2
-1
0
1
2
Height AGL, m
1800
1600
1400
1200
1000
800
600
400
11:00
11:15
11:30
11:45
12:00
Time, UTC

Figure 5. Same as Fig. 2 but for temperature, potential temperature, and detrended temperature fluctuations: time-height cross sections measured with the UHOH RRL on 24 April 2013 between 11:00 and 12:00 UTC. The temporal and spatial resolution of the data is $\Delta t = 10$ s and $\Delta z = 3.75$ m with a gliding average of 109 m. The instantaneous CBL heights determined with the Haar-wavelet analysis are marked (same as shown in Fig. 2). a.g.l.: above ground level. (~~White~~ Black vertical lines are ~~artefacts~~ gaps which ~~appear when bringing~~ result from gridding the ~~profiles on~~ data to exact 10 s intervals; these artefacts ~~are neglected within~~ do not influence the turbulence analysis.)

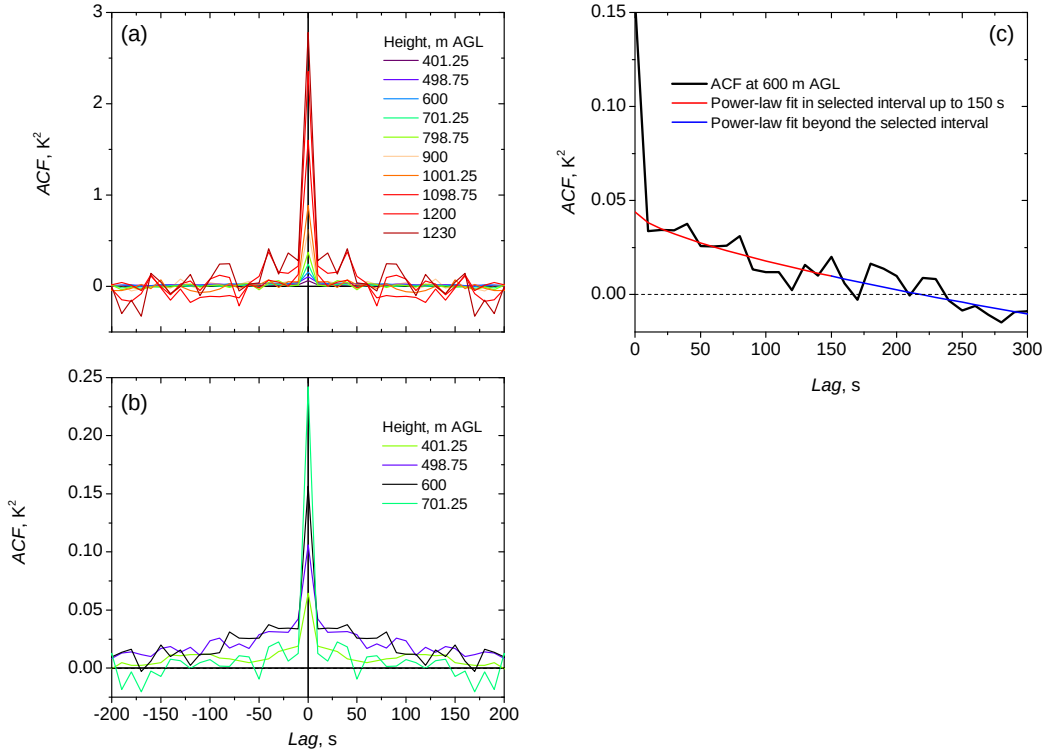

Figure 6. (a) Autocovariance functions (ACF) around the zero lag obtained at different heights from the temperature measurements shown in Fig. 5, i.e., with the data of 24 April 2013 between 11:00 and 12:00 UTC. (b) Zoom of (a) for lower heights only. (c) ACF with power-law fit for 600 m AGL.

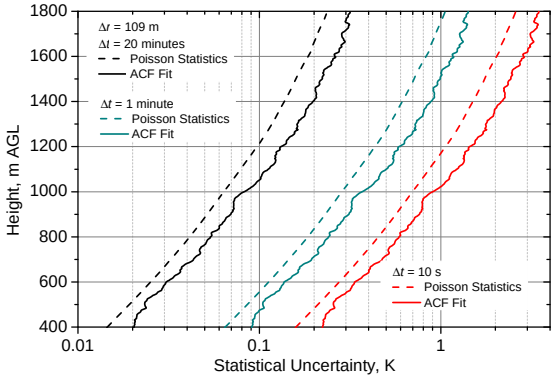

Figure 7. Statistical uncertainties of 10 s, 1 min, and 20 min temperature profiles at noontime determined with a $2/3$-power-law fit of the ACF data (see Fig. 6). ~~Statistical temperature uncertainties~~ Shot-noise errors calculated by use of Poisson statistics from the detected ~~photon number~~ signal intensities in each height are shown for comparison. It can be seen that the statistical uncertainty of the RRL temperature measurements is mainly governed by ~~Poisson statistics~~shot noise. The range resolution of the data was 109 m.

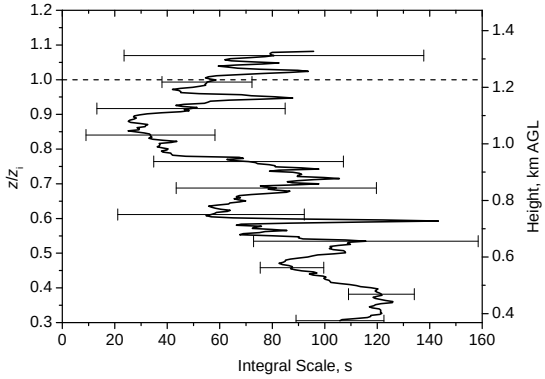

Figure 8. Integral scale of the temperature fluctuations shown in Fig. 5 (1 h period between 11:00 and 12:00 UTC, 24 April 2013). Error bars show the ~~remaining root-mean-square variation of the noise-corrected data~~noise errors. The mean CBL height z_i of 1230 m (dashed line) was determined with the Haar-wavelet analysis of β_{par} and was used for the relative height scale z/z_i. ~~Data around 0.9 and above 1.15 z/z_i were omitted because the data were too noisy here due to variances close to zero, see below.~~

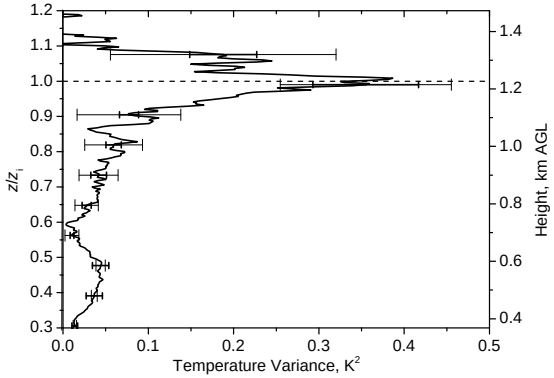

Figure 9. Profile of temperature variance (1 h period between 11:00 and 12:00 UTC, 24 April 2013). Error bars show the ~~remaining root-mean-square variability of the noise-corrected data~~ noise errors (thin error bars) and the sampling ~~error~~ errors (thick error bars). The mean CBL height z_i of 1230 m (dashed line) was used for the relative height scale z/z_i.

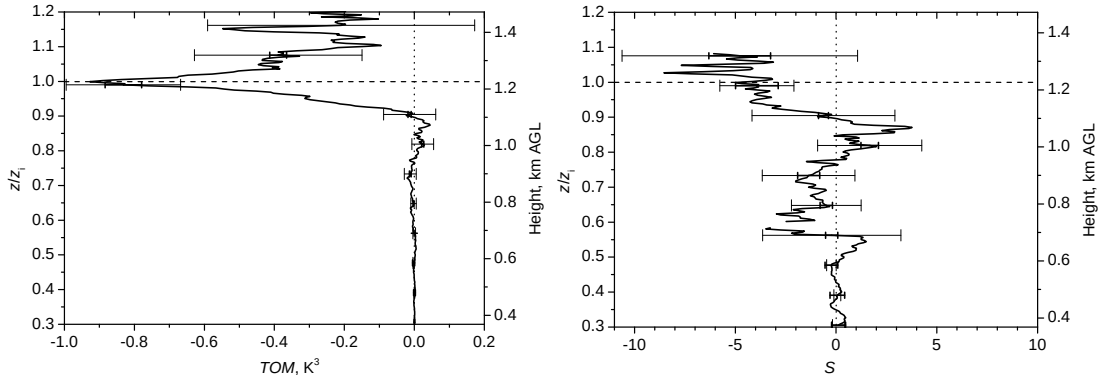

Figure 10. Same as Fig. 9 but profiles of the third-order moment (TOM) and the skewness S. Error bars show the ~~remaining root-mean-square variability of the noise-corrected data~~ noise errors (thin error bars) and the sampling ~~error~~ errors (thick error bars). The mean CBL height z_i of 1230 m (dashed line) was used for the relative height scale z/z_i. The dotted vertical line marks zero skewness. Skewness data around ~~0.9~~ 0.6 and above ~~1.15~~ 1.1 z/z_i were omitted because the data were too noisy here due to variances close to zero.

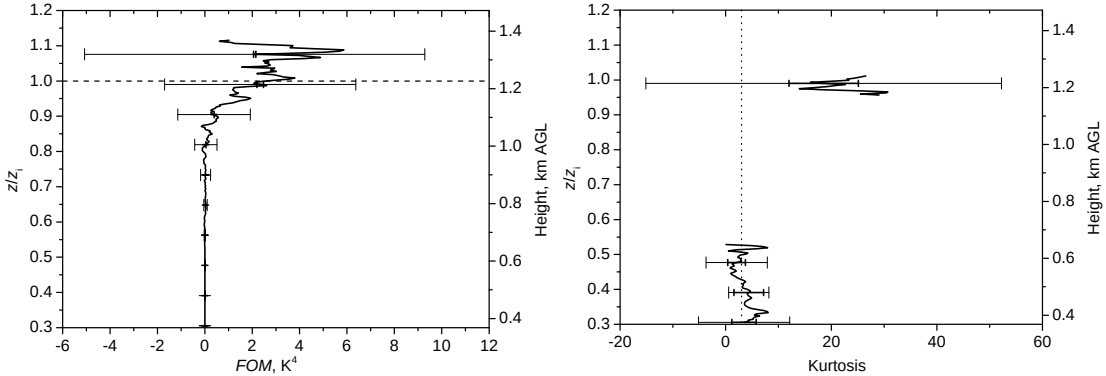

Figure 11. Same as Fig. 9 but profiles of the forth-order moment FOM and kurtosis. Only kurtosis data below ~~0.5~~ 0.55 and around 1.0 z/z_i are shown because other data are too noisy. The dotted vertical line in the lower panel marks a value of 3 which is the kurtosis of the normal distribution. Error bars show the ~~remaining root-mean-square variability of the noise-corrected data~~ noise errors (thin error bars) and the sampling ~~error~~ errors (thick error bars). The mean CBL height z_i of 1230 m (dashed line in the upper panel) was used for the relative height scale z/z_i.